Peer-reviewed version available at *Int. J. Mol. Sci.* **2020**, *21*, 469; doi:10.3390/ijms21020469

Article

Characterization Of Human Pluripotent Stem Cell-Derived Hepatocytes With Adult Features And Potential For Modeling Metabolic Diseases

Gustav Holmgren [1,†], Benjamin Ulfenborg [1,†,*], Annika Asplund [2], Karin Toet [3], Christian X Andersson [2], Ann Hammarstedt [4,‡], Roeland Hanemaaijer [3], Barbara Küppers-Munther [2,*] and Jane Synnergren [1]

[1] University of Skövde, Skövde, Sweden;
[2] Takara Bio Europe AB, Gothenburg, Sweden;
[3] TNO Metabolic Health Research, Leiden, The Netherlands;
[4] The Lundberg Laboratory for Diabetes Research, Departments of Molecular and clinical Medicine, Institute of medicine, Sahlgrenska Academy, University of Gothenburg, Gothenburg, Sweden;
* Correspondence: B.U.: benjamin.ulfenborg@his.se; B.K.-M.: barbara_kuppersmunther@takarabio.com
† These authors contributed equally to this work.
‡ Present address: AstraZeneca Gothenburg, BioPharmaceuticals R&D, Late-stage Development, Mölndal, Sweden

Abstract: There is a strong anticipated future for human pluripotent stem cell-derived hepatocytes (hiPS-HEP), but so far their use has been limited due to insufficient functionality. We investigated the potential of hiPS-HEP as an *in vitro* model for metabolic diseases by combining transcriptomics with multiple functional assays. The transcriptomics analysis revealed that 86% of the genes were expressed at similar levels in hiPS-HEP as in human primary hepatocytes (hphep). Adult characteristics of the hiPS-HEP were confirmed by the presence of important hepatocyte features, e.g. Albumin secretion and expression of major drug metabolizing genes. Normal energy metabolism is crucial for modeling metabolic diseases, and both transcriptomics data and functional assays showed that hiPS-HEP were similar to hphep regarding uptake of glucose, LDL and fatty acids. Importantly, the inflammatory state of the hiPS-HEP was low under standard conditions, but in response to lipid accumulation and ER stress the inflammation marker TNFα was upregulated. Furthermore, hiPS-HEP could be co-cultured with primary hepatic stellate cells both in 2D and in 3D spheroids, paving the way for using these co-cultures for modeling NASH. Taken together, hiPS-HEP have the potential to serve as an *in vitro* model for metabolic diseases. Furthermore, differently expressed genes identified in this study can serve as targets for future improvements of the hiPS-HEP.

Keywords: human pluripotent stem cells, human stem cell-derived hepatocytes, *in vitro*, metabolic diseases, transcriptomics, maturation, characterization

1. Introduction

The liver is an organ that spans a large variety of over 500 different functions in the body: energy metabolism, detoxification, and production of serum proteins and bile, just to mention a few. Consequently, liver disease or liver toxicity that cause impaired liver functionality have severe effects on normal body functions. Liver diseases are a major burden to the public health and estimations show a global liver-related mortality rate of approx. 2 million patients per year [1]. In addition, the liver is one of the organs with the highest susceptibility to drug toxicity, significantly contributing to the high attrition rates in current drug discovery processes [2]. Therefore, there is a strong need for better and more predictive *in vitro* models for liver disease and toxicity. A general opinion within the field of safety assessment and disease modeling is that *in vitro* cell models will increasingly contribute

to improve the mechanistic understanding of diseases and the prediction of adverse effects of drugs in humans in the future.

The gold standard for studying liver disease or hepatotoxicity *in vitro* are metabolically competent human primary hepatocytes (hphep), either freshly isolated or cryopreserved. However, the hphep have several shortcomings that limit their use. The shortage of relevant human donor material, the large donor variation, and the rapid loss of their functionality in culture [3-6], are the most prominent problems. Furthermore, the liver consists of multiple cell types; hepatocytes and non-parenchymal cells, such as cholangiocytes, endothelial cells, hepatic stellate cells, and Kupffer cells. As a consequence, an *in vitro* liver model with capacity to display all hepatic functions needs to consist of several if not all hepatic cell types and not only hepatocytes. In addition to using multiple cell types, a 3-dimensional (3D) culture environment is beneficial for an *in vitro* model as it allows the formation of cell-cell contacts and the formation of cell polarity in hepatocytes as indicated by the presence of bile canaliculi [7].

Nonetheless, functional hepatocytes will constitute the major part of a relevant *in vitro* liver model, and therefore, stem cell research has been focused on deriving mature hepatocytes from stem cells. Due to the many diverse features of hepatocytes, and also considering the fact that primary hepatocytes rapidly lose key functions when cultured in conventional 2D cultures *in vitro*, it is not surprising that hepatocytes are one of the most challenging cell type to derive from stem cells and further mature *in vitro*.

In order to explore the potential of a cell model and identify good-to-go areas for the cell model, a thorough characterization of the cells in question is necessary. This characterization needs to be done on multiple levels, preferably combining large-scale transcriptomics assessment with multiple functional assays [8]. Importantly, hepatocytes exist in periportal and perivenous phenotypes in the liver lobe, commonly known as metabolic zonation [9], and it is important to look at features for both these hepatocyte populations when assessing a hepatocyte cell model.

Human pluripotent stem cells (hiPSC) are an inexhaustible source of cells and have the potential to differentiate into specialized cell types, which provides unique opportunities for usage in a wide range of applications. The possibility to convert hiPSCs into functional hepatocytes allows for novel opportunities in assay development and holds great potential for future pre-clinical and regenerative medicine applications. For example, hiPSC derived from patients suffering from, e.g., inherited metabolic diseases can be used for modeling these types of diseases *in vitro* [10-12]. Combining the hiPSC technology with the constantly progressing genome editing technologies, e.g. CRISPR-Cas9, further increases the potential for disease modeling and therapeutic applications [13, 14].

The study presented here describes a thorough characterization of hiPSC-derived hepatocytes (hiPS-HEP), in order to assess their potential as *in vitro* tools for metabolism studies and disease modeling. The cells were subjected to a broad panel of characterization assays, ranging from transcriptomics analysis, protein expression, to multiple functional assays. The results show that the hiPS-HEP possess many adult hepatocyte features that can be maintained in conventional 2D cultures for over 2 weeks. The transcriptomics analysis revealed that a majority of genes (86%) are similarly expressed in all the three test groups. Taken together, this study highlights the potential of hiPSC-derived hepatocytes as a robust and reproducible source for hepatocyte-related *in vitro* models, e.g., metabolism-related liver diseases.

2. Results

In the present study, the maturation status and the functionality of the hiPS-HEP was compared to hphep by combining large-scale transcriptomics with multiple functional readouts covering a variety of important hepatocyte functions, as suggested by Schwartz et al [8] amongst others. In order to assess the reproducibility and robustness of the used differentiation protocol, two batches of hiPS-HEP derived from three different hiPSC lines were tested.

2. 1 Homogeneous population of hiPSC-derived hepatocytes with mature hepatocyte features

First, the expression of typical hepatocyte-related markers such as albumin (*ALB*), asialoglycoprotein receptor 1 (*ASGPR1*), connexin 32 (*GJB1*), hepatocyte nuclear factor 4α (*HNF4α*), and α1-antitrypsin (*AAT*) was investigated in hiPS-HEP and these markers were found to be expressed at similar mRNA levels as in hphep (Figure 1A; for hphep donor demographics see Table 1). As expected, the mRNA expression of these five markers decreased in the hphep after culturing for 24 hours (hphep d0 vs d1).

Next, protein expression of these hepatocyte markers was investigated using immunocytochemistry (ICC; Figure 1C, D). Almost all cells in the hiPS-HEP and hphep cultures were immuno-positive for HNF4α (Figure 1C1 and C5, respectively; Suppl. Figure 1). Quantification using CellC Cell Counting software showed that more than 92% of the cells in hiPS-HEP cultures derived from the three hiPSC lines ChiPSC12, ChiPSC18 and ChiPSC22 expressed HNF4α, counted in relation to DAPI staining (Suppl. Figure 1). The few HNF4α-negative cells are also likely to be derived from DE since these cultures are near-homogenous with 97% Sox17-immunopositive cells [18].

In contrast to the homogenous HNF4α expression, ASGPR1, α1-Antitrypsin (AAT), and Albumin (Alb) appeared to be more strongly expressed in a subpopulation in both hiPS-HEP and hphep cultures (Figure 1C2-C4 and 1C6-8, respectively). The immunostaining of these three markers was very similar for hiPS-HEP derived from all three hiPSC lines (Suppl. Figure 1).

In agreement with *Albumin* mRNA expression levels and immunostainings, Albumin secretion was found to be at similar levels in hiPS-HEP and hphep (Figure 1D). Importantly, Albumin secretion by hiPS-HEP was stable for over two weeks in culture (between day 4 and 20 post-thaw) indicating phenotypical stability. In order to evaluate urea secretion, another important liver specific function, the mRNA expression levels of key enzymes of the urea cycle and other related genes were compared in hphep and hiPS-HEP. Several urea cycle-related genes were expressed at similar mRNA levels in hiPS-HEP compared to hphep (Figure 1B), whereas *ARG1*, *ASL*, *ASS1*, *CPS1*, *OTC* and *SLC25A2* were expressed at significantly lower levels in hiPS-HEP compared to hphep directly after thawing (d0). When measuring urea secretion upon ammonium challenge, hiPS-HEP displayed lower urea secretion than hphep cultured for 1 day post-thaw (d1; Figure 1E) which may be due to the lower expression of *ARG1* in hiPS-HEP compared to hphep d1 (Figure 1B). Similarly, to the stable Albumin secretion, urea secretion was stable in hiPS-HEP between day 13 and 20 post-thaw (Figure 1E).

Preprints (www.preprints.org) | NOT PEER-REVIEWED | Posted: 14 November 2019 doi:10.20944/preprints201911.0162.v1

Peer-reviewed version available at Int. J. Mol. Sci. 2020, 21, 469; doi:10.3390/ijms21020469

127

Figure 1

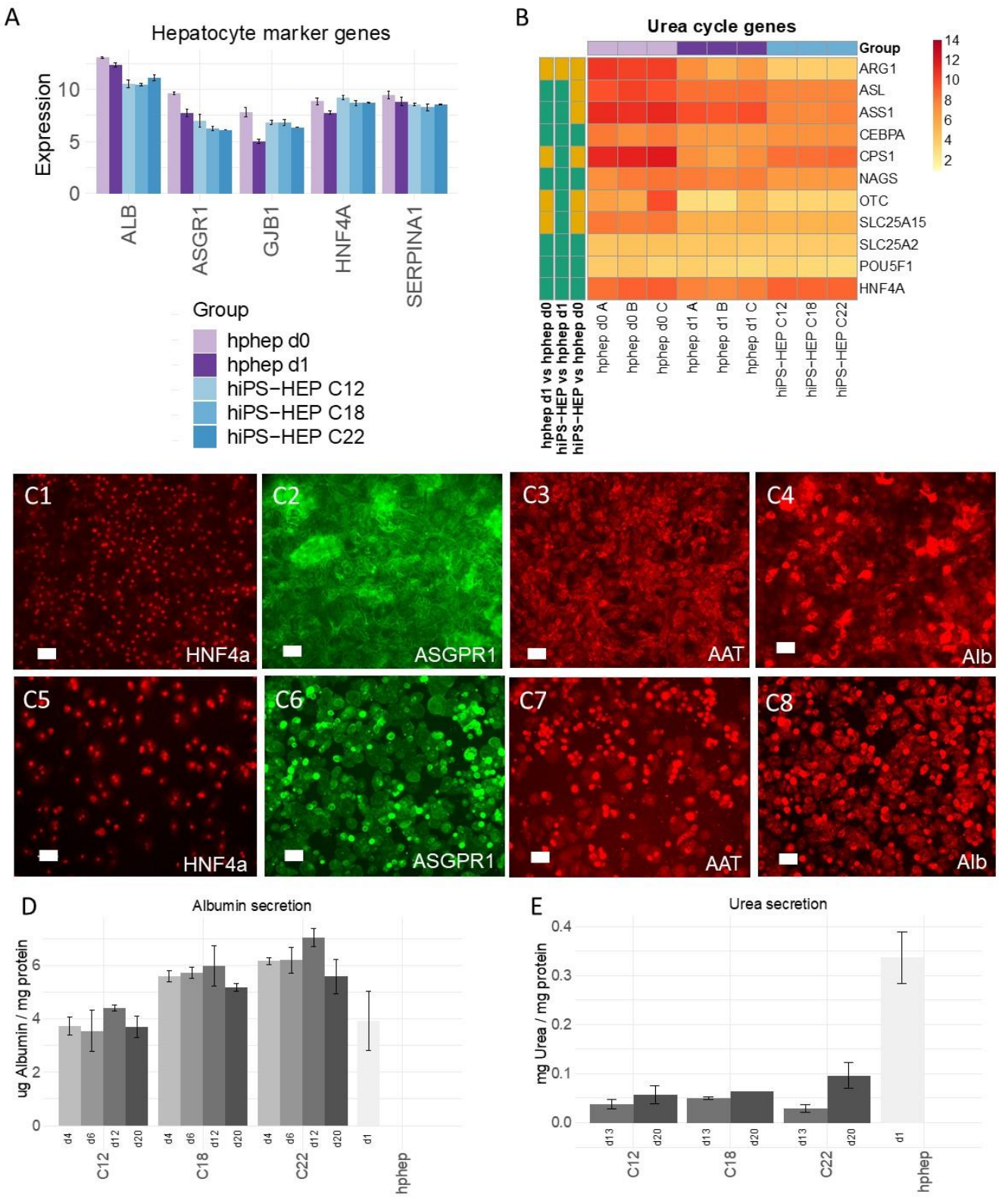

128

129 **Figure 1: Expression of general hepatocyte markers and functions in hiPS-HEP**

130 A) mRNA expression of the general hepatocyte markers albumin (*ALB*), asialoglycoprotein receptor 1

131 (*ASGPR1*), connexin 32 (*GJB1*), hepatocyte nuclear factor 4α (*HNF4α*), and α1-antitrypsin (*AAT*) in hiPS-

HEP derived from three hiPSC lines (ChiPSC12, ChiPSC18, ChiPSC22) on day 13 post-thawing and hphep directly after thawing (d0) and on day 1 post-thawing (d1). Error bars represent standard deviation of different cell batches for hiPS-HEP (n=2 batches) and different donors for hphep (n=3 donors), respectively. B) Heatmap of mRNA expression of urea cycle genes in hiPS-HEP derived from three hiPSC lines (ChiPSC12, ChiPSC18, ChiPSC22) on day 13 post-thawing and hphep directly after thawing (d0) and on day 1 post-thawing (d1). The panel to the left of the heatmap indicates significant differences between the groups (adj. P-value < 0.05, absolute log2 fold change > 2; green = no significant difference, orange = significant difference). C) Representative pictures of ICC stainings of the hepatocyte markers Hepatocyte Nuclear Factor 4α (HNF4α), Asialoglycoprotein receptor 1 (ASGPR1), α1-Antitrypsin (AAT), and Albumin (Alb) in hiPS-HEP derived from ChiPSC18 on day 12 post-thawing (C1-4) and hphep cultured for 24 hours (C5-8). Scale bars 50µm. D) Albumin secretion in hiPS-HEP derived from three hiPSC lines (ChiPSC12, ChiPSC18, ChiPSC22) on days 4, 6, 12 and 20 post-thaw compared to hphep cultured for one day (d1) post-thaw. Error bars represent standard deviation of duplicate wells per group. E) Urea secretion in hiPS-HEP derived from three hiPSC lines (ChiPSC12, ChiPSC18, ChiPSC22) on days 13 and 20 post-thaw compared to hphep cultured for one day (d1) post-thaw. Error bars represent standard deviation of duplicate wells per group.

Table 1. Donor demographics of the human primary hepatocytes

Donor	Age	Gender	Ethnicity	Cause of death	Viability
KFF	56	male	Caucasian	anoxia, 2nd to cardiac arrest	95%
YEM	46	female	Caucasian	intracerebral hemorrhage - stroke	87%
MSW	69	male	African-American	intracerebral hemorrhage, 2nd to cerebrovascular accident (stroke)	91%

2.2 Expression of drug metabolizing enzymes and transporters

Expression and functionality of the drug metabolizing machinery, comprising phase I and phase II enzymes as well as transporter proteins, is of critical importance for the utility of an *in vitro* hepatocyte model in drug metabolism and hepatotoxicity studies but of less importance for disease modeling. Since several enzymes are known to be specific for fetal or adult hepatocytes, analyses of these enzymes can also aid to assess the grade of maturity of the cells.

We started by investigating the most important Cytochrome P450 (CYP) enzymes and found that several CYP enzymes were expressed in hiPS-HEP at similar mRNA levels as in hphep d1, e.g., *CYP2C19, 2C9, 3A4, 3A5*, and *3A7* (Figure 2A). In contrast to that, other enzymes such as *CYP1A2, CYP2B6,* and *CYP2D6*, were expressed at lower levels in hiPS-HEP compared to hphep d1 (Figure 2A). Importantly, the similar levels of the adult enzyme *CYP3A4* and the fetal enzyme *CYP3A7* in hiPS-HEP and hphep indicate an adult feature of hiPS-HEP. Since a low correlation between mRNA and activity levels for many phase I and II enzymes as well as transporters has been reported by Ohtsuki et al [15], we also assessed the enzyme activity levels by incubating with specific substrates for the different enzymes and measuring the formation of the specific metabolites with LC/MS. We found that hiPS-HEP had similar CYP1A, CYP3A, and CYP2C9 activities as hphep cultured for 20 h (including the activity assay; Figure 2D1-3). In contrast, CYP2B6 and CYP2D6 activity levels were lower in hiPS-HEP compared to hphep (Figure 2D) which is in agreement with the mRNA expression (Figure 2A). Notably, CYP activities in hiPS-HEP were stable or even increasing for a period of 14 days, between day 4 and 19 (Figure 2D1-6). A discrepancy between CYP2C19 and CYP2C9 mRNA and activity levels could be observed. *CYP2C19* mRNA expression is on the same level in the two cell types, whereas the activity is approximately 10 times lower in hiPS-HEP than in hphep (Figure 2A and D6). However, the LC/MS method does not seem to be as stable for detection of the CYP2C19 metabolite as for the other metabolites. Regarding CYP2C9, lower mRNA levels were observed in hiPS-HEP than in hphep but the activity levels were similar in both cell models (Figure 2A and D3). The discrepancies seen between mRNA and activity levels for some CYP enzymes are not unexpected. Ohtsuki et al. have reported previously that CYP2C9 and CYP2C19 are among the CYP

177 enzymes with the lowest correlation between mRNA and activity levels [15]. This clearly emphasizes
178 that protein expression or preferably functional assays are essential when characterizing *in vitro*
179 hepatocyte models.
180 Since drug metabolism is also performed by phase II enzymes, we investigated the expression
181 of two classes of phase II enzymes, sulfotransferases (SULT) and UDP-glucuronosyl transferases
182 (UGT). All tested SULTs and UGTs were found to be expressed on similar mRNA levels between the
183 two cell types (Figure 2B). In agreement with that, incubations with the substrate 7-OH-coumarin
184 revealed similar or higher SULT and UGT activity levels in hiPS-HEP and in hphep cultured for 20 h
185 (including the activity assay; Fig 2E and F). Similarly to the CYP activities, phase II enzyme activities
186 were stable or even increasing in hiPS-HEP during a 14-day culture period (between day 4-19 post-
187 thaw).
188 Besides phase I and II enzymes, transporter proteins play an important role in xenobiotics
189 metabolism. Therefore, we also investigated the mRNA expression of 19 transporters, including both
190 uptake and efflux transporters. 11 transporters were expressed on similar levels in both cell types,
191 e.g., *ABCC2* (MRP2) and *SLC10A1* (NTCP), whereas eight were expressed at lower levels in hiPS-
192 HEP, e.g., *ABCB11* (BSEP) and *SLCO1B1* (OATP1B1; Figure 2C). The protein expression of MRP2,
193 NTCP, BSEP, and OATP1B1 were confirmed by immunostainings (Figure 2G1-4).
194

Preprints (www.preprints.org) | NOT PEER-REVIEWED | Posted: 14 November 2019 doi:10.20944/preprints201911.0162.v1

Peer-reviewed version available at *Int. J. Mol. Sci.* **2020**, *21*, 469; doi:10.3390/ijms21020469

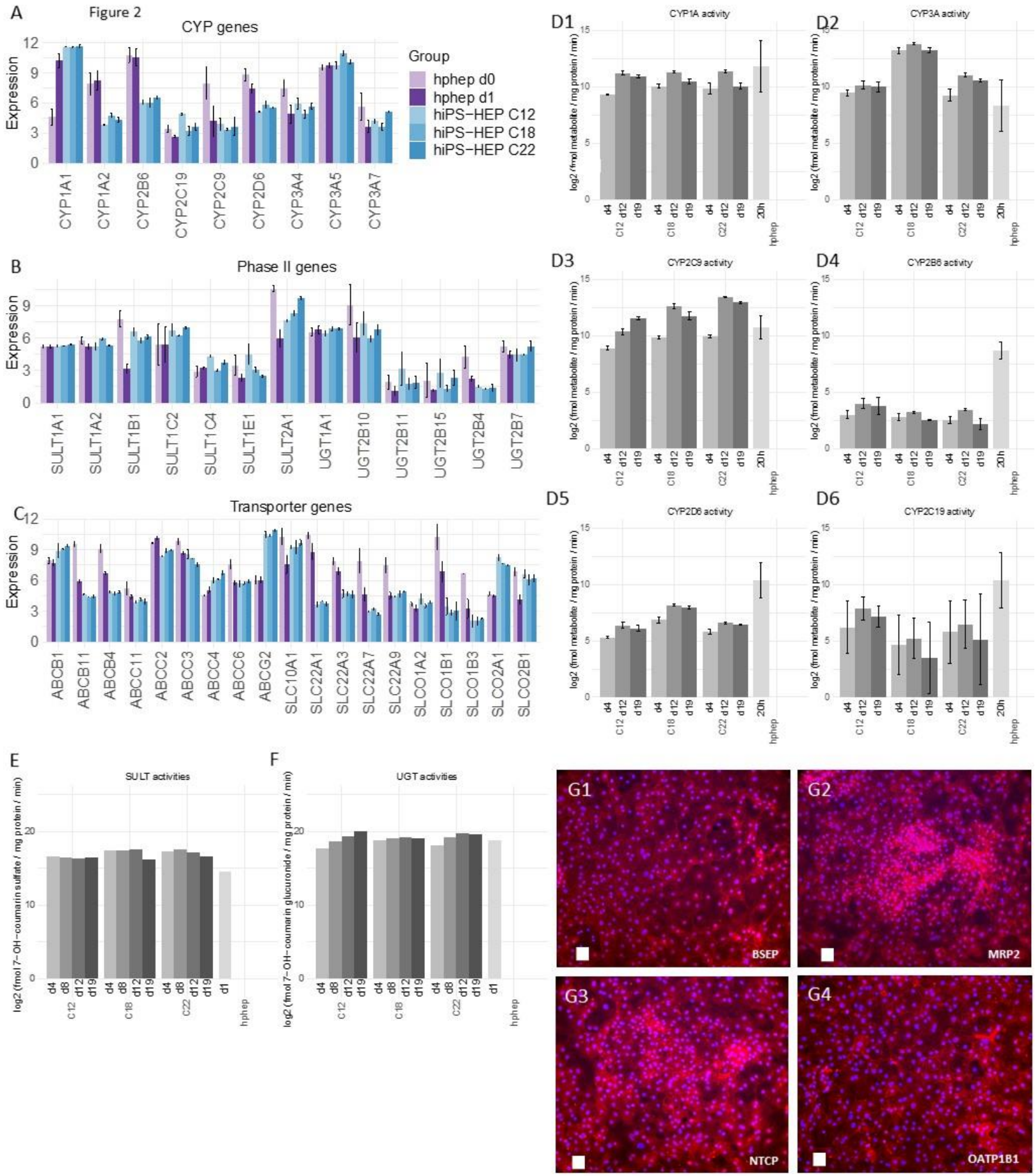

195

Figure 2: Expression of genes of the drug metabolizing machinery in hiPS-HEP
A-C) mRNA expression of nine cytochrome P450 enzymes (A), 13 phase II enzymes (B) and 19 transporter proteins (C) in hiPS-HEP derived from three hiPSC lines (ChiPSC12, ChiPSC18, ChiPSC22) on day 13 post-thawing and hphep directly after thawing (d0) and on day 1 post-thawing (d1). Error bars represent standard deviation of different cell batches for hiPS-HEP (n=2 batches) and different donors for hphep (n=3 donors), respectively. D) Enzyme activities of CYP1A (D1; metabolite: Paracetamol), CYP3A (D2; metabolite: OH-Midazolam), CYP2C9 (D3; metabolite: OH-Diclofenac), CYP2B6 (D4; metabolite: OH-Bupropion), CYP2D6 (D5; metabolite: OH-Bufuralol), and CYP2C19 (D6; metabolite: OH-Mephenytoin) in hiPS-HEP derived from three hiPSC lines (ChiPSC12, ChiPSC18, ChiPSC22) on days 4, 12 and 19 post-thaw compared to hphep cultured for 20 hours (20h) post-thaw as measured by LC/MS. Error bars represent standard deviation of different cell batches for hiPS-HEP (n=2 batches) and different donors for hphep (n=3 donors), respectively. E-F) Enzyme activities of the phase II enzymes Sulfotransferases (E; metabolite: 7-OH-coumarin sulfate) and UDP-glucuronosyl transferases (F; metabolite: 7-OH-coumarin glucuronide) in hiPS-HEP derived from three hiPSC lines (ChiPSC12, ChiPSC18, ChiPSC22) on days 4, 8, 12 and 19 post-thaw compared to hphep cultured for one day (d1) post-thaw as measured by LC/MS. Data for hphep are mean values of three different donors. hiPS-HEP samples were pooled from two individual wells. G) Representative pictures of ICC stainings of the transporters Bile Salt Export Pump (BSEP, ABCB11), Multidrug resistance-associated protein 2 (MRP2, ABCC2), Na+-taurocholate co-transporting polypeptide (NTCP, SLC10A1), and organic anion transporting polypeptide 1B1 (OATP1B1, SLCO1B1) in hiPS-HEP derived from ChiPSC18 on day 12 post-thawing (G1-4). Nuclear counterstaining with DAPI. Scale bars 50µm. Abbreviations: CYP: Cytochrome P450; DAPI: 4′,6-diamidino-2-phenylindole; LC/MS: liquid chromatography/mass spectrometry, SULT: sulfotransferases, UGT: UDP-glucuronosyl transferases.

2.3 Glucose metabolism and insulin signaling

Another important and rapidly growing area of use for hepatocytes is disease modeling. For example, hepatocytes are crucial for modeling metabolic functions performed by the liver and for diseases such as non-alcoholic fatty liver disease (NAFLD) and non-alcoholic steatohepatitis (NASH) which are global, rapidly growing problems. In order to evaluate the utility of hiPS-HEP for modeling NAFLD/NASH, we started by investigating the energy metabolism of glucose and lipids as well as insulin signaling and inflammation in the hiPS-HEP.

First, we compared the mRNA expression of more than 40 genes central in glucose metabolism in hiPS-HEP and hphep and found the vast majority to be expressed at similar levels in both cell types (Figure 3A). Only eight of the genes were significantly differently expressed between hiPS-HEP and hphep d0 and/or d1. The genes expressed at lower levels in hiPS-HEP were fructose-1,6-biphosphatase 1 (*FBP1*), glutamic-oxaloacetic transaminase 1 (*GOT1*), pyruvate carboxylase (*PC*) and phosphoenolpyruvate carboxykinase 1 (*PCK1*), compared to hphep d0. On the other hand, Glycerol-3-phosphate dehydrogenase (*GPD2*), glycogen synthase 1 (*GYS1*), Oxoglutarate Dehydrogenase (*OGDH*), and hexokinase 2 (*HK2*) showed higher mRNA expression levels in hiPS-HEP compared to hphep d0 and/or d1. Interestingly, *PC, PCK1, FBP1, GOT1*, and *GPD2* are directly involved in gluconeogenesis, and *OGDH* has a strong influence on 2-oxoglutarate, which regulates the gluconeogenesis in the liver [31]. Noteworthy is that *PC, PCK1, and FBP1* were also significantly lower expressed in hphep d1 than in hphep d0.

One important hepatocyte function in glucose metabolism is the ability to synthesize and store glycogen (glycogenesis). Therefore, periodic acid Schiff (PAS) staining was performed on both hiPS-HEP at day 12 after thaw and on hphep at day 1 after thaw. As shown in figure 3C1-3, glycogen was detected in a subset of hiPS-HEP (derived from all three hiPSC lines). Similarly, hphep also showed glycogen storage in a subpopulation of the cells (Fig, 3C4). The presence of glycogen is in agreement with the finding that several key enzymes of glycogenesis are well expressed in hiPS-HEP: Hexokinase (*HK*), UDP-glucose pyrophosphorylase (*UGP2*), glycogen synthase (*GYS*), and Glycogen branching enzyme (*GBE1*; Figure 3A).

Another essential feature of metabolically functional hepatocytes is the physiological response to insulin. Thus, the mRNA expression of 19 genes involved in insulin signaling were compared in hiPS-HEP and hphep and no significant differences in expression levels of these 19 genes were found

between the two cell types (Figure 3B), including key genes such as insulin receptor (*INSR*), insulin receptor substrate 1 and 2 (*IRS1*, *IRS2*), and AKT serine/threonine kinases 1 and 2 (*AKT1*, *AKT2*). In order to test if the hiPS-HEP respond to an insulin stimulus by phosphorylation of AKT kinase which is a key regulator in the insulin signaling cascade, the hiPS-HEP were incubated for 3 hours in an insulin-free medium followed by an incubation for 10 minutes with 100nM insulin. In the insulin-treated cells, a significant increase of phosphorylated AKT could be detected compared to untreated control cells, while the total AKT content was similar in treated and untreated cells, as shown by Western Blot (Figure 3D).

Figure 3

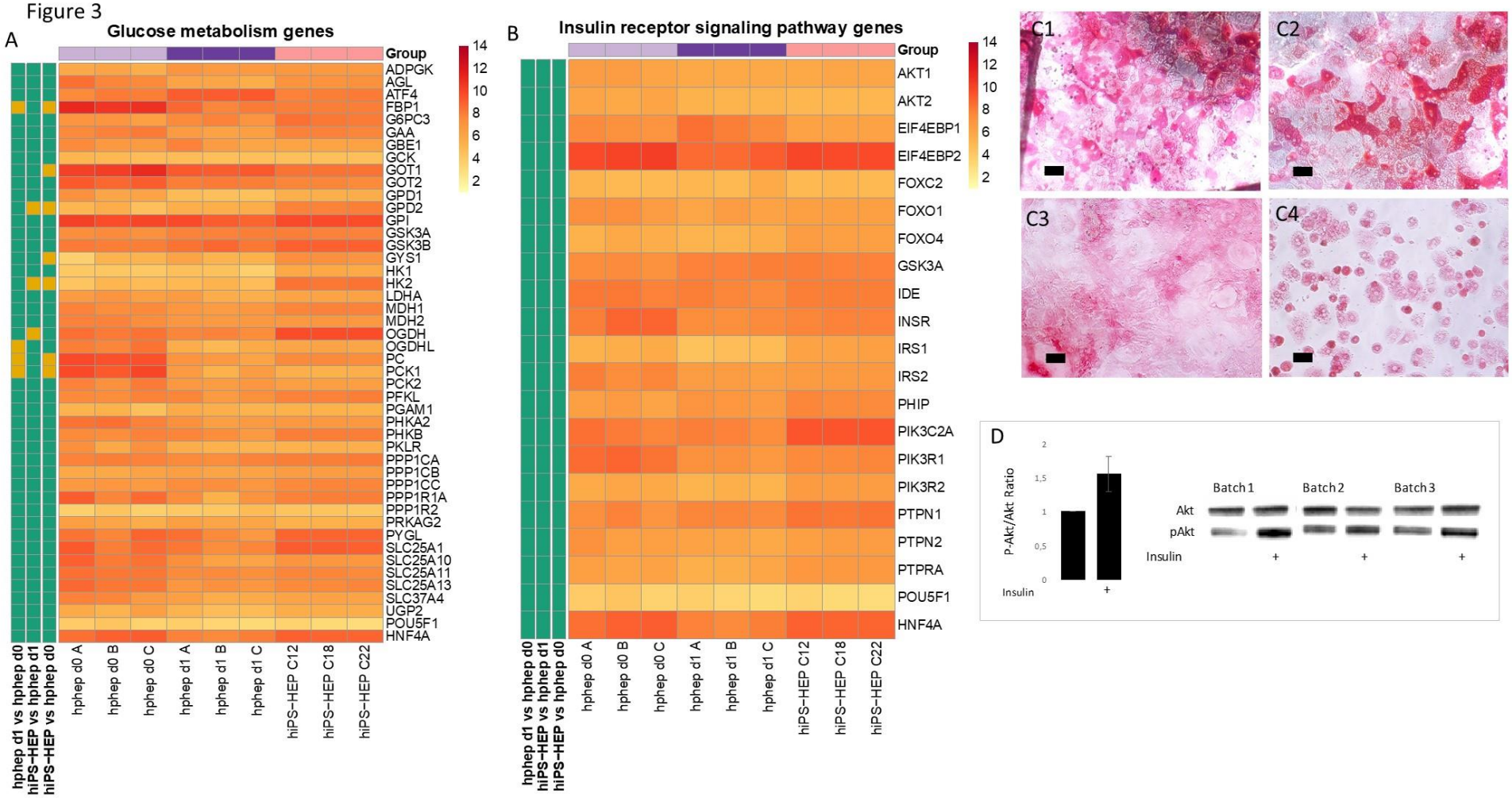

Figure 3: Glucose metabolism and Insulin receptor signaling in hiPS-HEP

A-B) Heatmap of mRNA expression of genes involved in glucose metabolism (A) and insulin signaling (B) in hiPS-HEP derived from three hiPSC lines (ChiPSC12, ChiPSC18, ChiPSC22) on day 13 post-thawing and hphep directly after thawing (d0) and on day 1 post-thawing (d1). The panel to the left of the heatmap indicates significant differences between the groups (adj. P-value < 0.05, absolute log2 fold change > 2; green = no significant difference, orange = significant difference). C) Representative pictures of Periodic acid Schiff staining of Glycogen deposition in hiPS-HEP derived from ChiPSC12 (C1), ChiPSC18 (C2), and ChiPSC22 (C3) on day 12 post-thawing and hphep cultured for 24 hours (C4). Scale bars 50µm. D) Western blot detection of AKT and phosphorylated AKT (pAKT) in hiPS-HEP after a 10 min incubation with and without 100 nM Insulin, respectively. The ratio of pAKT and total AKT was calculated for three batches of hiPS-HEP derived from ChiPSC18 on day 12 post-thawing and is presented as fold change compared to the control cells without Insulin stimulation. Error bars represent standard deviation of different cell batches for hiPS-HEP (n=3 batches).

2.4 Cholesterol and lipid metabolism

Next, we assessed the mRNA expression levels of 29 genes involved in cholesterol metabolism and 47 genes involved in fatty acid metabolism in both hiPS-HEP and hphep. The vast majority of the cholesterol metabolism-related genes assessed were expressed at similar levels in hiPS-HEP and hphep, e.g., LDL receptor (*LDLR*) and *PCSK9* (Figure 4A). Only four of the investigated genes differed significantly between hiPS-HEP and hphep d0/1: ATP citrate lyase (*ACLY*) and apolipoprotein A1 and A4 (*APOA1; APOA4*), which were higher in hiPS-HEP, and apolipoprotein A5 (*APOA5*) which was lower expressed in hiPS-HEP (Figure 4A). Noteworthy, the important gene *APOB* is expressed on similar level in hiPS-HEP and hphep d0. Next, we tested if the hiPS-HEP were capable of taking up fluorescently labeled Low Density Lipoprotein (LDL-DyLight). Already after a 3-hour incubation, accumulation of LDL-DyLight could be observed in the cells (Figure 4C) and an even stronger accumulation could be seen after 24 hours (data not shown).

The assessment of 48 genes involved in fatty acid metabolism revealed that only three genes were expressed at different levels in hiPS-HEP and hphep d0 (Figure 4B). The exceptions were acetyl-CoA carboxylase beta (*ACACB*) and bile acyl-CoA synthetase (*SLC27A5*), which were both expressed at lower levels in hiPS-HEP, and protein kinase AMP-activated catalytic subunit alpha 2 (*PRKAA2*), which was expressed at higher levels in hiPS-HEP than in hphep d0. Additionally, three genes were significantly different in hiPS-HEP compared to hphep d1; *HACD3* and *PECR* (both higher in hiPS-HEP); and *PPARD* (lower in hiPS-HEP). Noteworthy, *PECR* was also higher in hphep d1 compared to hphep d0, and *PPARD* and SLC27A5 were also lower in hphep d1 compared to hphep d0.

Preprints (www.preprints.org) | NOT PEER-REVIEWED | Posted: 14 November 2019 doi:10.20944/preprints201911.0162.v1

Peer-reviewed version available at *Int. J. Mol. Sci.* **2020**, *21*, 469; doi:10.3390/ijms21020469

Figure 4

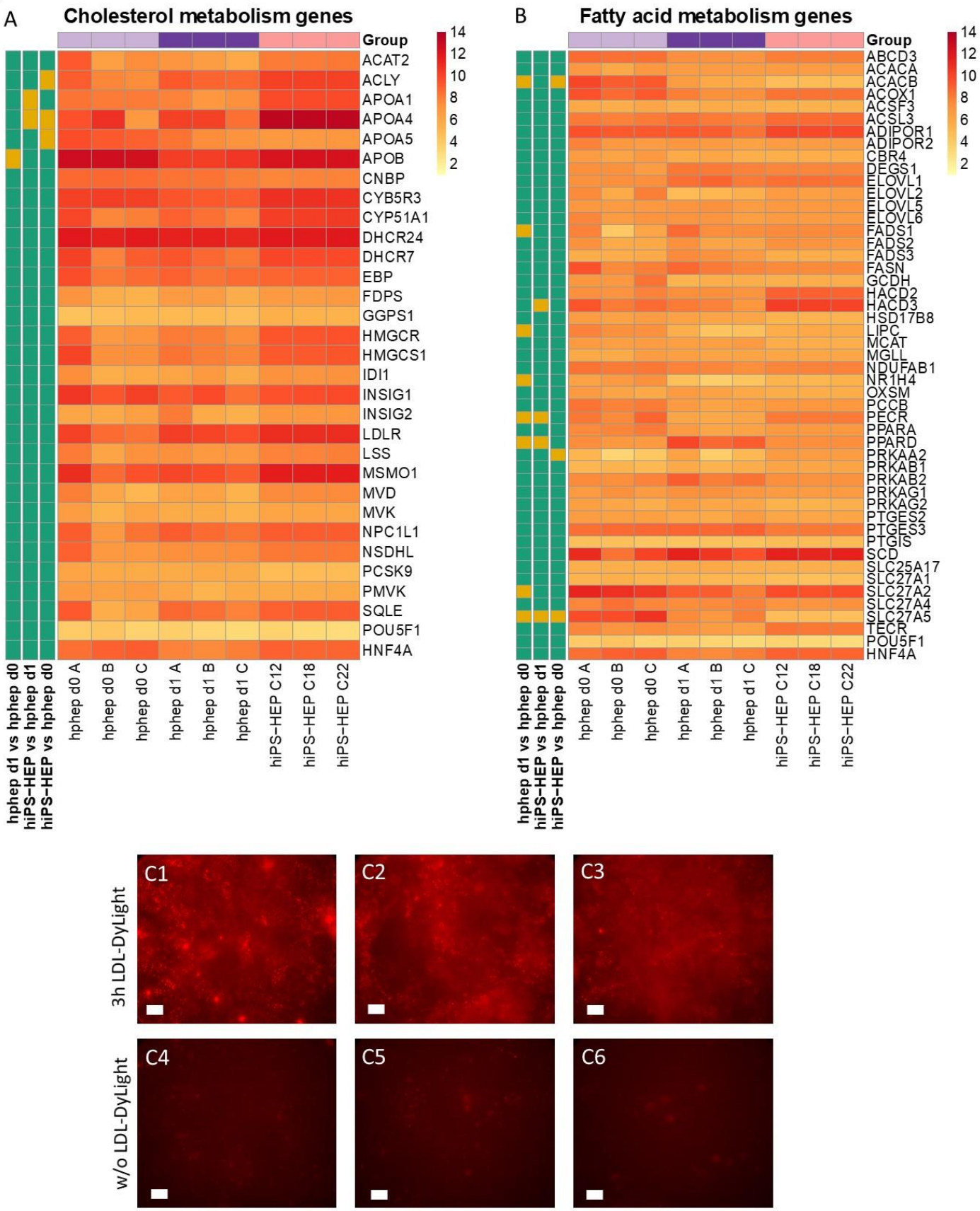

Figure 4: Lipid metabolism in hiPS-HEP

A-B) Heatmap of mRNA expression of genes involved in cholesterol metabolism (A) and fatty acid metabolism (B) in hiPS-HEP derived from three hiPSC lines (ChiPSC12, ChiPSC18, ChiPSC22) on day 13 post-thawing and hphep directly after thawing (d0) and on day 1 post-thawing (d1). The panel to the left of the heatmap indicates significant differences between the groups (adj. P-value < 0.05, absolute log2 fold change > 2; green = no significant difference, orange = significant difference). C) Representative pictures of hiPS-HEP derived from ChiPSC12 (C1, C4), ChiPSC18 (C2, C5), and ChiPSC22 (C3, C6) on day 12 post-thawing after three hours incubation with LDL-DyLight (C1-3) or untreated control cells (C4-6). Scale bars 50µm. Abbreviation: LDL: Low-density lipoprotein.

2.5 Inflammatory response and induction of steatosis

Many genes involved in inflammatory response are expressed by hepatocytes and are of interest for disease modeling. Figure 5A shows the expression levels of 72 inflammation-related genes in hiPS-HEP and hphep d0/1. Noteworthy, most inflammation-related genes are expressed at low or medium levels in both hiPS-HEP and hphep d0/1, e.g., caspase 4 (*CASP4*), tumor necrosis factor (*TNF*), Toll like receptor 1, 3, 4 (*TLR1, TLR3, TLR4*) which may indicate a healthy, non-inflammatory status of both cell types under standard conditions (Figure 5A). However, a few genes are expressed at high levels in both cell types, e.g., *AIMP1, ATRN, F11R, ITCH, MIF, PLAA, PRDX5*, and *RELA*.

When comparing expression levels between hiPS-HEP and hphep d0/1, we found the majority of the genes to be similarly expressed (Figure 5A) which is similar to previous results (Figure 3, 4). Only 12 out of the 72 genes differed significantly in expression levels between the two cell types: *CCL16, CRP, FOS, LTBR*, and *ORM1* were lower expressed in hiPS-HEP, whereas *AXL, CYBA, F2R, F2RL1*, and *RIPK2* were expressed at higher levels in hiPS-HEP.

Inflammation in the liver can, amongst others, be caused by fat accumulation. At first, fat is accumulated in the hepatocytes, a condition known as NAFLD, which can progress to NASH which is characterized by steatosis, inflammation, and fibrosis [16]. To model these conditions *in vitro*, one prerequisite is that hepatocytes can take up free fatty acids and store as lipid droplets. Therefore, we incubated hiPS-HEP for 24 hours with either 200 µM or 600 µM oleic acid (OA; coupled to fatty acid free BSA) or with fatty acid free BSA alone as vehicle control. Subsequently, the cells were stained for lipid accumulation using Oil Red O. Only few lipid droplets were observed in the control cells (Figure 5B1) while the cells incubated with 200µM OA and 600µM OA showed a dose dependent increase in lipid droplets (Figure 5B3 and 5B4, respectively). When we combined 200µM OA with 1µM Thapsigargin, a compound known to cause ER stress and to worsen steatosis [11], a clear increase of lipid accumulation was observed compared to only 200µM OA (Figure5B2 and 5B3, respectively).

Next, we investigated if inducing steatosis by treatment with OA and Thapsigargin caused an inflammatory response in the hiPS-HEP. Indeed, we found that the mRNA expression of the inflammatory marker tumor necrosis factor α (*TNFα*) was upregulated in OA/Thapsigargin-treated hiPS-HEP (Figure 5C). The strongest upregulation of *TNFα* was caused by 600µM OA, followed by the combination of 200µM OA and Thapsigargin compared to vehicle control (Figure 5C). Thus, this indicated that treatment with OA and Thapsigargin caused an inflammatory response.

Preprints (www.preprints.org) | NOT PEER-REVIEWED | Posted: 14 November 2019 doi:10.20944/preprints201911.0162.v1

Peer-reviewed version available at *Int. J. Mol. Sci.* **2020**, *21*, 469; doi:10.3390/ijms21020469

333

Figure 5

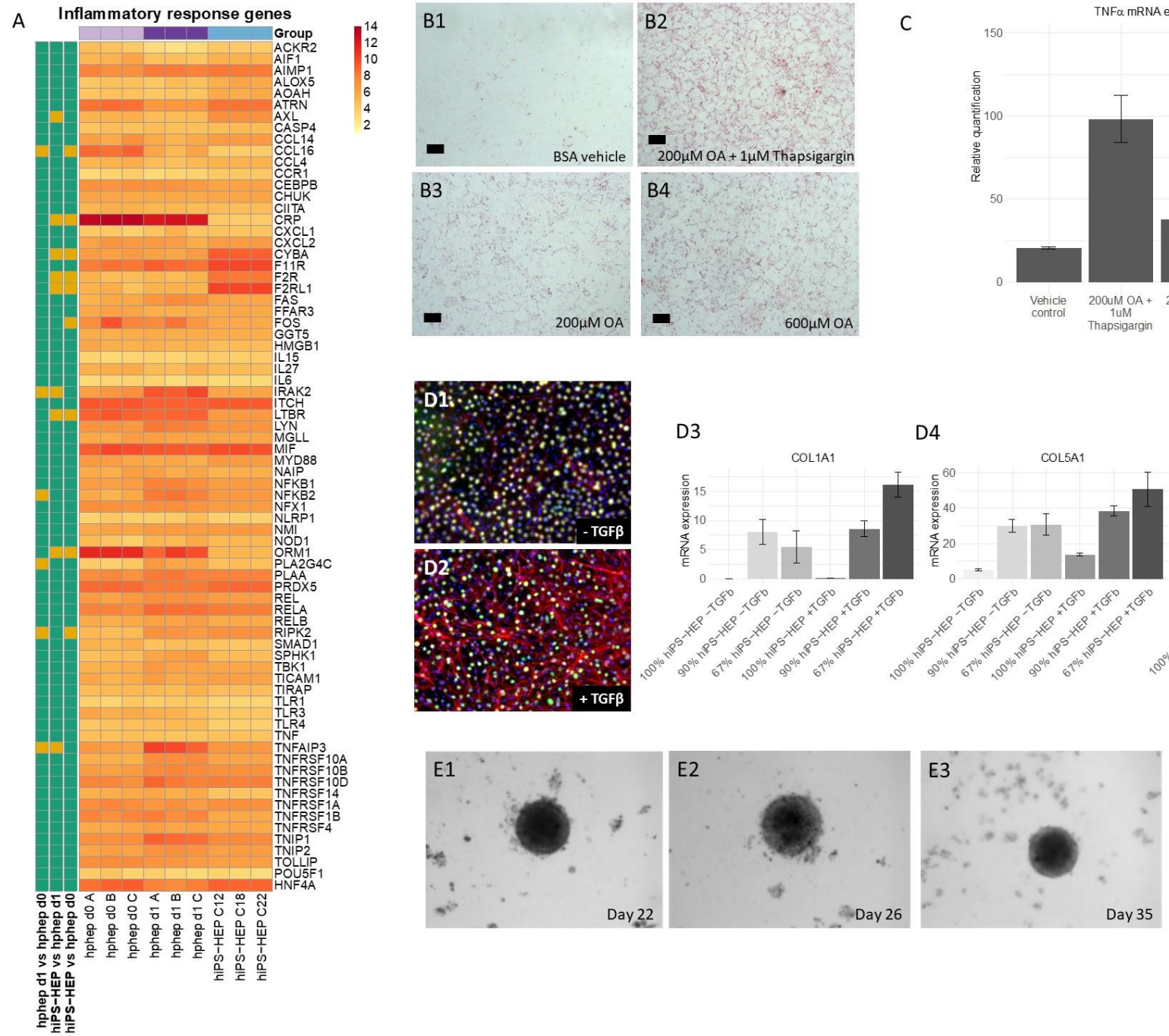

334

335 **Figure 5: Inflammatory response in hiPS-HEP and co-cultures of hiPS-HEP and primary HSC for NASH**
336 **modeling**

337 A) Heatmap of mRNA expression of genes involved in the inflammatory response in hiPS-HEP derived
338 from three hiPSC lines (ChiPSC12, ChiPSC18, ChiPSC22) on day 13 post-thawing and hphep directly after
339 thawing (d0) and on day 1 post-thawing (d1). The panel to the left of the heatmap indicates significant
340 differences between the groups (adj. P-value < 0.05, absolute log2 fold change > 2; green = no significant
341 difference, orange = significant difference). B) Representative stainings of hiPS-HEP on day 6 post-thaw

derived from ChiPSC18 with Oil Red O visualizing lipid accumulations after a 24 hour incubation with BSA vehicle (B1), 200µM OA and 1µM Thapsigargin (B2), 200µM OA (B3) and 600µM OA (B4), respectively. Scale bars 100µm. C) *TNFα* mRNA expression in hiPS-HEP on day 6 post-thaw derived from ChiPSC18 after a 24 hour incubation with BSA vehicle, 200µM OA and 1µM Thapsigargin, 200µM OA, and 600µM OA, respectively. D1-2) Representative pictures of HNF4α (green) and α-SMA (red) immunostainings of co-cultures of hiPS-HEP derived from ChiPSC18 and hepatic stellate cells (HSC) without (D1) and with (D2) a 4 day treatment with 20ng/ml TGFβ, respectively. Nuclear counterstaining with DAPI. D3-5) *Collagen 1A1* (D3), *Collagen 5A1* (D4), and *HNF4α* (D5) mRNA expression in cultures consisting of 100% hiPS-HEP : 0% HSC, 90% hiPS-HEP : 10% HSC, or 67% hiPS-HEP : 33% HSC with and without a 4 day treatment with 20ng/ml TGFβ, respectively. Error bars represent standard deviation of technical quadruplicates. E) Representative pictures of 3D spheroids consisting of hiPS-HEP and HSC (ratio 2:1) cultured for 22 days (E1), 26 days (E2), and 35 days (E3), respectively. Abbreviations: α-SMA: α-smooth muscle actin; DAPI: 4',6-diamidino-2-phenylindole; HNF4α: Hepatocyte Nuclear Factor 4α; HSC: hepatic stellate cells; OA: Oleic acid; TGFβ: transforming growth factor β; TNFα: Tumor necrosis factor α.

2.6 Co-cultures of hiPS-HEP and hepatic stellate cells for modeling NASH

In the advanced stage of NASH, fibrosis occurs in the liver, which is characterized by collagen deposited by activated hepatic stellate cells (HSC). Thus, for modeling NASH-related liver fibrosis, one needs to co-culture hepatocytes and HSC. Therefore, we adapted the culture conditions in a way that allowed co-culturing primary human HSC together with hiPS-HEP. In order to activate HSC, we treated the co-cultures with 20ng/ml TGFβ for 4 days which strongly increased the protein expression of α-SMA (Figure 5D2), a characteristic marker for activated HSC, compared to untreated cultures (Figure 5D1). HNF4α immunostainings were comparable in controls and TGFβ-treated cultures, indicating no major effect of TGFβ treatment on the hiPS-HEP cell density (Figure 5D1-2).

Since activated HSC are known to express collagens, we investigated collagen mRNA expression in the co-cultures after TGFβ treatment. In accordance with the observed increase in α-SMA expression upon TGFβ stimulation (Figure 5D2), we also observed increased *Collagen 1a1* and *5a1* mRNA expression in the TGFβ-treated co-cultures compared to hiPS-HEP cultures without HSC (Figure 5D3,4). Monocultures of hiPS-HEP alone showed no *Collagen 1a1* expression irrespective of treatment (Figure 5D3), whereas *Collagen 5a1* was expressed in untreated hiPS-HEP monocultures and upregulated upon TGFβ treatment, however at lower levels than in the co-cultures (Figure 5D4). As expected, *HNF4α* mRNA expression was lower in co-cultures than in the hiPS-HEP monocultures and was not affected by TGFβ treatment of the hiPS-HEP monocultures (Figure 5D5).

Taken together, the co-cultures responded as expected to TGFβ treatment with activation of the HSC and upregulation of α-SMA and collagen expression. However, already the untreated control co-cultures displayed a weak α-SMA immunostaining (Figure 5D1) which indicated that a subpopulation of the HSC was already activated. This is in agreement with previous reports that HSC get activated in 2D cultures due to the stiff matrix [17]. In order to avoid the HSC activation due to the 2D culture setting, we generated spheroids of hiPS-HEP and HSC. To this end, we seeded hiPS-HEP and HSC in ultra-low attachment plates, spheroids formed within 1-2 days and could be maintained for at least 35 days (Figure 5E1-3). In future studies, the utility of the co-culture spheroids for NAFLD and NASH studies can be explored.

2.7 Similarities and differences between hiPS-HEP and hphep

To further assess the similarities and differences between hiPS-HEP and hphep on gene expression level, a global analysis of the transcriptomics data was carried out. Figure 6A depicts the number of transcripts that are similarly expressed, with a coefficient of variation (CV) < 0.1, throughout all samples between the different comparisons. A great majority of the transcripts (24,685 transcripts, 86 %) are similarly expressed across all group comparisons. Not surprisingly, the highest number of similarly expressed genes (27,157) in the different sample group comparisons is found in hphep d0 vs hphep d1. hiPS-HEP show a comparable number of similarly expressed genes when compared to hphep d1 and hphep d0 (26,492 and 26,244, respectively).

Using a generalized linear model (GLM) and the criterion described in the method section, in total 2,866 differentially expressed genes (DEGs) were detected as significant in at least one of the sample group comparisons. Figure 6B displays the overlap of DEGs between the three group comparisons. Out of these DEGs, only 76 genes are differentially expressed between all sample group comparisons. 2,655 genes are differentially expressed when comparing hiPS-HEP to hphep, either at day 0 or day 1 (Figure 6B, A2-A7). Approximately 25% of these genes are also differentially expressed between hphep at day 1 and hphep at day 0 (Figure 6B, A2, A4, A6). To assess the biological relevance of the DEGs, a pathway over-representation analysis was carried out on the different groups of DEGs according to the overlapping areas (A1-A7) in figure 6B. For a complete list of significant over-represented pathways, see Supplemental table 1. Among the 76 DEGs that differ between all three groups (Figure 6B, A4) there is an over-representation for pathways such as, "Cytochrome P450 – arranged by substrate type", "CYP2E1 reactions", "Phase I – Functionalization of compounds", "Phase II – Conjugation of compounds", as well as pathways related to bile acids and bile salts. These pathways are also over-represented in the comparison between hphep d1 and hphep d0 (Figure 6B, A1), as well as in the overlap between hphep d1 vs hphep d0 and hiPS-HEP vs hphep d0 (Figure 6B, A2, A4). The genes *CYP2E1*, *CYP4A11*, and *CYP2C8*, associated with the CYP P450 pathways, have the following expression rank between the groups: hphep d0 > hphep d1 > hiPS-HEP. The same expression pattern is seen for the bile acid/bile salts related genes (SLC27A5, SLCO1B1, AKR1C4). The genes associated with "Phase II – Conjugation of compounds" have a more ambiguous expression, *ACSM5*: hphep d0 > hphep d1 > hiPS-HEP, *SULT2A1*: hphep d0 > hiPS-HEP > hphep d1, and *UGT2A3*: hiPS-HEP > hphep d0 > hphep d1.

The DEGs in hiPS-HEP compared to hphep d1 (Figure 6B, A7) show an over-representation for "Attenuation phase" and "HSP1-dependent transactivation"; the associated genes are *HSPA1A*, *HSPA1B*, *DNAJB1*, with the ranking hphep d1 > hphep d0 > hiPS-HEP, and *CAMK2D* with an opposite expression ranking. When comparing hiPS-HEP to hphep d0 (Figure 6B, A3), hiPS-HEP show a higher expression of genes related to glycogen synthesis and metabolism. For the comparison hphep d0 vs hiPS-HEP and hphep d1 vs hiPS-HEP (Figure 6B, A5), the pathways "Laminin interactions", "Non-integrin membrane-ECM interactions", "ECM proteoglycans", and "Extracellular matrix organization" are over-represented with the expression ranking hiPS-HEP > hphep d1 > hphep d0. The DEGs in hphep d1 when compared to hiPS-HEP or hphep d0 (Figure 6B, A6), are overrepresented in pathways related to respiratory electron transport and the citric acid cycle.

Figure 6

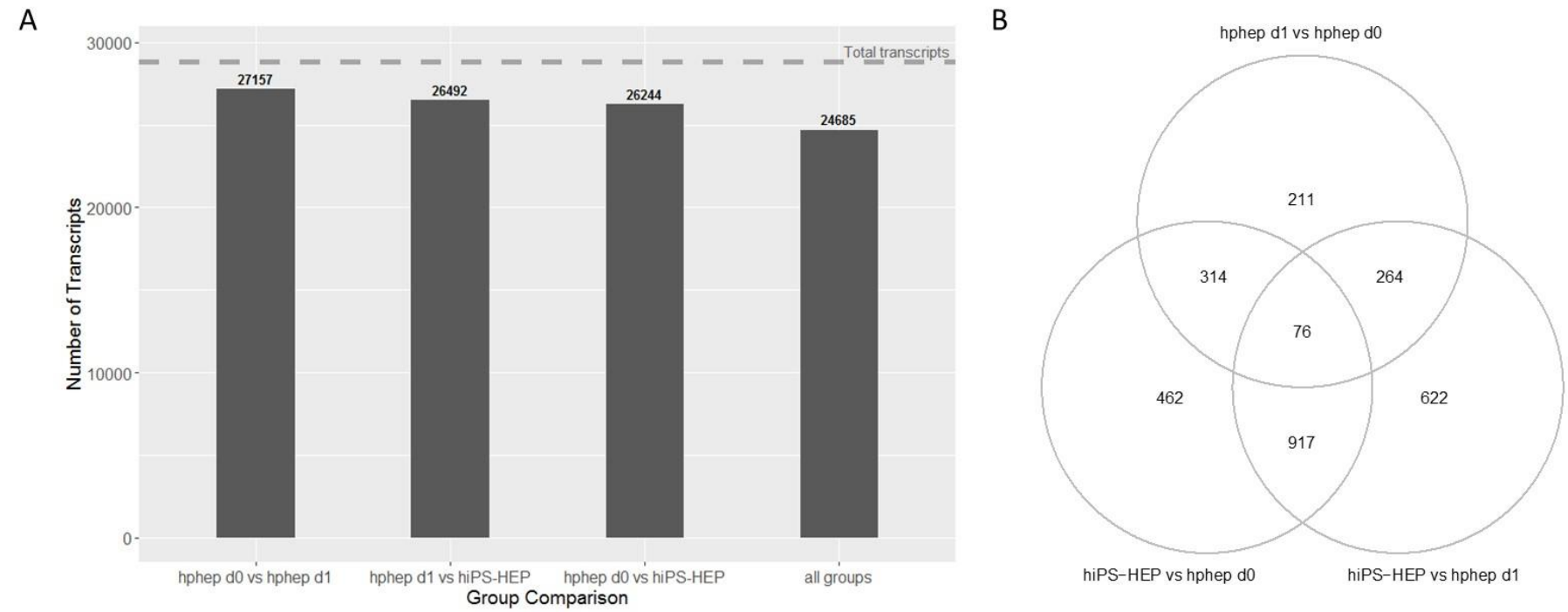

Figure 6: Global gene expression analysis of transcriptomics data

A) Number of similarly expressed mRNA transcripts for the different group comparisons. B) Venn diagram of 2,866 differentially expressed genes (DEGs) between the different group comparisons: hphep d0 vs hphep d1 (area A1), hphep d0 vs hiPS-HEP (area A3), hphep d1 vs hiPS-HEP (area A7), hphep d0 vs hphep d1 and hphep d0 vs hiPS-HEP (area A2), hphep d0 vs hiPS-HEP and hphep d1 vs hiPS-HEP (area A5), hphep d0 vs hphep d1 and hphep d1 vs hiPS-HEP (area A6), and all three groups (area A4).

3. Discussion

The present study covers an in-depth characterization of hiPSC-derived hepatocytes including multiple phenotypic and functional aspects of relevance for several application areas, for example modeling of metabolic disease.

An essential requirement for the utility of stem cell-derived hepatocytes for all application areas is that homogenous hepatocyte cultures can be robustly derived from large panels of stem cell lines. To evaluate the homogeneity of the hiPS-HEP cultures, we stained for the key hepatocyte transcription factor HNF4α and found that it was expressed in 92% of hiPS-HEP cells, thus indicating a highly efficient differentiation result. An equally high differentiation efficiency, 93.8% HNF4α-positive cells, was obtained when we screened a panel of 25 lines using an earlier version of the hepatocyte differentiation protocol used in this study to derive hiPS-HEP [18]. Notably, the hepatocyte differentiation protocol worked for all lines without any modifications. In contrast to our findings, others have reported that their protocols either do not work for some hPSC lines making it necessary to select lines that appear more prone to differentiate into hepatocytes [19], or that they require time- and labor-intensive adaptations of the protocol for individual lines [20]. One great advantage of the hiPSC technology is the possibility to generate iPSC lines from many different donors, healthy and diseased, so that one can recreate the population diversity *in vitro*. However, this requires differentiation protocols that, without adaptations, generate homogeneous cultures from virtually all lines.

Besides high homogeneity, the reproducibility of the differentiation protocol is of great importance so that different cell batches show the same characteristics. We found that different hiPS-HEP batches derived from the same hiPSC line showed overall little variation; see for example expression of hepatocyte markers (Figure 1A), expression of the drug metabolizing machinery (Figure 2A-C), CYP activity results (Figure 2D) and insulin signaling (Figure 3D).

In contrast to the homogenous HNF4α-expression in hiPS-HEP, other markers or features are expressed only in a subpopulation of both hiPS-HEP and hphep, e.g., Albumin, α1-Antitrypsin, ASGPR1, and glycogen storage (Figure 1). One would expect to find such different populations of hepatocytes since this is well-described for the liver and known as metabolic zonation [9]. In the liver lobe, hepatocytes exist in periportal and perivenous phenotypes and therefore, it is important to look at features for both populations, e.g., albumin expression (predominantly in periportal hepatocytes) and CYP expression (predominantly in perivenous hepatocytes), when assessing a hepatocyte cell model. However, we cannot rule out that the observed heterogeneity for maturation markers such as Albumin and ASGPR1 in the hiPS-HEP cultures could be due to different levels of maturity.

We assessed the maturation status of the hiPS-HEP by performing transcriptomics analysis and functional assays in comparison to adult human primary hepatocytes. Albumin secretion, which is one hallmark for adult hepatocytes, was on similar levels in hiPS-HEP and hphep (Figure 1D) which was confirmed by similar *Albumin* mRNA levels in both cell types (Figure 1A). Another characteristic of adult hepatocytes is high expression of the adult enzymes *CYP3A4* and low expression of the fetal enzyme *CYP3A7* which was the case in both cell types (Figure 2A). ASGPR1, a marker for stem cell-derived hepatocytes enriched for primary hepatocyte features [21], showed also similar mRNA levels and immunostainings in hiPS-HEP and hphep (Figure 1A, C2, C6) which suggested that hiPS-HEP have several adult hepatocyte features at levels comparable to hphep.

Two functionalities that require further improvement in hiPS-HEP are, 1) urea secretion and 2), the drug metabolizing machinery, comprising phase I and II enzymes as well as transporters. Urea secretion was clearly lower in hiPS-HEP than in hphep d1 (Figure 1E). The only urea cycle gene that was lower in hiPS-HEP than in hphep was *ARG1* (Figure 1B) which is the last in the chain of five key enzymes in the urea cycle [22] and is likely the cause of the restricted urea production. Regarding phase I enzymes, the three main CYP enzymes, CYP1A, 3A and 2C9, had similar activity levels in hiPS-HEP and in hphep d1. CYP1A, 3A and 2C9 combined metabolize about 60% of prescription drugs (CYP3A4 37%; CYP1A2 9%; CYP2C9 17%; [24]), but in order to be useful for drug metabolism studies all enzymes need to be expressed at useful levels. Therefore, expression of CYP2B6, 2D6 and 2C19 needs to be improved in hiPS-HEP (Figure 2D). We observed a similar situation for transporters as for the CYP enzymes: some were well expressed, e.g. MRP2 (*ABCC2*) and NTCP (SLC10A1) and some need to be increased in hiPS-HEP, e.g. *OATP1B1* and *OATP1B3* (Figure 2C). Regarding phase II metabolism, we focused on UGTs and SULTs since they are responsible for more than half of all phase II metabolism of clinically used drugs [25] and found SULT and UGT activity levels to be similar in hiPS-HEP and hphep (Figure 2E-F).

Noteworthy, Albumin and urea secretion as well as CYP and phase II activities were stable over time in hiPS-HEP (Figure 1D-E; Figure 2D, E-F). This phenotypic stability of the hiPS-HEP is clearly a superior feature over hphep, which are known to quickly loose functions such as CYP activities in conventional 2D cultures [27, 30]. Many studies, for example for hepatitis virus studies and toxicity studies with repeated dosing, require a chronic treatment and a culture period of at least 2 weeks which is why phenotypic stability is of great importance for an *in vitro* hepatocyte model.

As expected, hphep display large variations of CYP activities between donors (see error bars for hphep in Figure 2D) which reflect the large inter-individual variation existing in the population (see e.g., [15]). This variation is a major issue that researchers are facing when using primary hepatocytes for *in vitro* models since the amount of hphep from one donor is limited and researchers are therefore forced to switch to new donors that may have a very different phenotype potentially affecting their studies. Therefore, one main advantage of hiPS-HEP is that one can obtain virtually unlimited amounts of cells from one donor, and importantly, there is only very low variation between different batches of hiPS-HEP, as seen for example in the reproducible and robust expression of hepatocyte

markers (Figure 1A), drug metabolizing genes (Figure 2A-C), CYP activities (Figure 2D), and the response to insulin (Figure 3D). Noteworthy, inter-individual variation in the CYP activity profile can be observed when comparing hiPS-HEP derived from different iPSC lines: e.g., hiPS-HEP derived from ChiPSC18 have higher CYP3A and 2D6 activities than the other 2 lines (Figure 2D2,5), which is likely due to higher expression of the polymorphic genes CYP3A5 and 2D6 in ChiPSC18 (Figure 2A).

Energy metabolism is another key function of the liver. The results presented here indicate that hiPS-HEP have a similar glucose and lipid metabolism as hphep, the gold standard (Figures 3-4). However, several genes related to gluconeogenesis, e.g., *PC, PCK1, FBP1, GOT1, GPD2* and *OGDH*, are expressed on lower levels in hiPS-HEP (Figure 3A). A potential cause could be the relatively high glucose concentration in the culture medium which would also explain the downregulation of gluconeogenesis-related genes in hphep d1 compared to hphep d0 (Figure 3A).

One important area of use for hepatocytes is to model NAFLD, a common cause for chronic liver disease with a prevalence of 20-30% in Europe [33]. NAFLD can progress to NASH which is associated with a higher risk of liver-related mortality and cardiovascular disease [34], and further to cirrhosis with an increased risk for hepatocellular carcinoma [35]. The long progression until clinical signs, the lack of good diagnostic tools as well as the absence of relevant preclinical models hampers the development of adequate treatments and drugs for NADFL/NASH, and highlights the need for novel translational *in vitro* models [36]. Several animal models have been developed, however, due to the heterogeneous pathology few or none of these models represent the human situation accurately [37]. Therefore, there is great and urgent need for an *in vitro* model for NAFLD/NASH.

Our data presented here suggest that hiPS-HEP could serve as such a potential NAFLD/NASH model. Most genes related to lipid and cholesterol metabolism are expressed at similar levels as in hphep d0/1 (Figure 4). Only four genes differed significantly between hiPS-HEP and hphep d0/1, for example *APOA5*, which is involved in lipoprotein metabolism by interacting with LDL receptor [38]. However, despite the lower *APOA5* expression in hiPS-HEP and in agreement with substantial expression of the *LDL receptor*, we found that hiPS-HEP accumulated labelled LDL upon a short incubation (Figure 4A,C). We also observed dose-dependent steatosis, which in turn lead to dose-dependent upregulation of the inflammatory marker *TNFα* (Figure 5B-C). Importantly, under standard culture conditions most inflammation related genes were expressed at similarly low levels both in hphep and hiPS-HEP (Figure 5A), indicating a healthy status of the cells and no activation of an inflammatory response which is a prerequisite for the utility of the hiPS-HEP for modelling inflammation. Furthermore, hiPS-HEP responded in the anticipated manner to Thapsigargin-induced ER stress [11, 39], with both an increased lipid accumulation and an upregulated *TNFα* expression (Figure 5B-C). Taken together, these results indicate that hiPS-HEP are similar to adult primary hepatocytes regarding glucose and lipid metabolism as well as inflammatory markers. The observed responses are essential for a relevant human *in vitro* model for NAFLD/NASH and highlight the potential use of hiPS-HEP for such models. Another important finding is that key drug targets for NAFLD/NASH treatment are well expressed in hiPS-HEP, e.g. the peroxisome proliferator−activated receptor-α (*PPARA*) and -δ (*PPARD*), which are targets for the elafibranor [40], and the nuclear receptor FXR (*NR1H4*), which is a target for obeticholic acid [41]. All three genes are expressed on the same level in hiPS-HEP and hphep d0 (Figure 4B) which demonstrates the potential of hiPS-HEP for drug target studies for NAFLD/NASH.

Since the progression of NAFLD to NASH includes a contribution of inflammatory and fibrogenic response from non-parenchymal cells, hepatocytes need to be co-cultured with non-parenchymal cells, such as stellate cells and Kupffer cells, as reviewed in [37]. To date, only a limited number of attempts using primary cells or cell lines (reviewed in [42]) or hepatocytes derived from human pluripotent stem cells [11, 43] have been reported in the NASH field. However, in the two NASH studies utilizing stem cell-derived hepatocytes, those were not co-cultured with non-parenchymal cells [11, 43]. Two other studies described 2D co-cultures of several hiPSC-derived liver cell types: liver progenitor cells and HSC [44], and liver progenitor cells, liver sinusoidal endothelial cells and HSC [45], respectively, and reported a positive effect of the co-culture on the maturity of the hiPSC-liver progenitor cells but did not evaluate the utility of the co-cultures for modeling NASH.

Another study reported modeling of liver fibrosis using the hepatoma cell line HepaRG and hiPSC-derived HSC [46]. To the best of our knowledge, our study is the first one to describe co-cultures of hiPSC-derived hepatocytes and human primary HSC. Importantly, we found that α-SMA expression, a hallmark of activated HSC and fibrosis, was induced in HSC in 2D co-cultures by TGFβ treatment. Since HSC showed a weak activation in 2D even without TGFβ stimulation, we generated 3D-spheroids of hiPS-HEP and HSC which can be maintained for at least 35 days. The results presented here pave the way for further exploring the utility of these co-culture spheroids for NASH studies. The 3D co-culture setting may even further improve the hiPS-HEP functionality compared to 2D cultures, similarly to reports on 3D spheroids consisting of hphep and non-parenchymal cells [7].

The global analysis of the transcriptomics data revealed very similar phenotypes of the three cell populations (Figure 6A). Differences were observed, amongst others, in phase I and II metabolism, indicating a lower functionality of hiPS-HEP and hphep d1 compared to hphep d0, which is in line with our gene expression and functional data on drug metabolism (Figure 2). Interestingly, in the DEGs between hiPS-HEP and hphep d0 and d1 "Attenuation phase" and "HSP1-dependent transactivation" are over-represented pathways which are related to cellular response to heat stress. It has been reported previously that cryopreservation and re-plating of hphep results in reduced ability to form cell-matrix and cell-cell interactions which triggers stress and heat shock responses [47]. Our observation that DEGs involved in these pathways (*HSPA1A, HSPA1B*, and *DNAJB1*) are upregulated in hphep d0 and d1 compared to hiPS-HEP is in line with these reports. Furthermore, pathways connected to ECM and laminin interactions are over-represented in the DEGs between hiPS-HEP and hphep d0 and d1, with higher expression in hiPS-HEP. A possible explanation could be that hiPS-HEP are differentiated in 2D cultures whereas hphep come from a 3D environment. It would be interesting to investigate if these pathways are downregulated in hiPS-HEP 3D spheroids.

The identification of DEGs is of great importance since they can provide a basis for future improvements as the aim is to reach the same functionality and maturity in hiPS-HEP as in hphep d0. One incentive for such continuous efforts is that hphep are not useful as a cell source for gene editing and are limited for disease modeling of a specific genetic background. The advance of the hiPSC technology allows to routinely generate hiPSC lines from many individuals, including healthy persons and patients, and thus represent the whole population. Furthermore, genetic modification of hiPSC lines using for example CRISPR/Cas9, allows to study the molecular basis of diseases.

Taken together, the hiPS-HEP used in this study represent a homogenous cell population with a high similarity to hphep and a potential for modeling NAFLD/NASH. Our results highlight the great promise of hiPSC-derived hepatocytes as an unlimited cell source to build more advanced cell models, to better recapitulate the human liver environment, to reflect the population diversity and to increase the predictability for disease modeling.

4. Materials and Methods

Cell culture

Cryopreserved hiPS-HEPs derived from the hiPSC lines ChiPSC12, ChiPSC18, and ChiPSC22 were thawed, plated and maintained according to the vendor instructions (Cellartis Enhanced hiPS-HEP v2 kits, Cat.no. Y10133, Y10134, Y10135, Takara Bio, www.takarabio.com). Enhanced hiPS-HEP v2 were maintained for up to 21 days post-thawing with media changes every 2 or 3 days using the Cellartis Enhanced hiPS-HEP Long-Term Maintenance Medium included in the kits.

For 2D co-cultures of Enhanced hiPS-HEP v2 and primary human stellate cells (HCS, BioIVT, Brussels, Belgium), cells were seeded on a Fibronectin coating (concentration 2µg/cm2; Roche, Basel, Swiss) in a 2:1 ratio (hiPS-HEP: HSC) at a cell density of 400K/cm2 using the regular plating medium included in the hiPS-HEP v2 kits. Instead of the regular HEP Long-Term Maintenance Medium the following maintenance medium was used for the co-cultures: Williams' Medium E supplemented with 0.1% PEST (15140-130, ThermoFisher), 0.5% DMSO (D2650, Sigma), 0.67% Cellartis Hepatocyte supplement (Y11149, Takara Bio), 2% Cellartis Hepatocyte Additives (Y11078, Takara Bio), 194µM L-

Proline (P5607, Sigma), and 173µM L-ascorbic acid 2-phosphate sesquimagnesium salt (A8960, Sigma).

For 3D co-cultures of Enhanced hiPS-HEP v2 and HSC, cells were seeded in a 2:1 ratio (hiPS-HEP: HSC) in InVitroGRO CP medium (BioIVT) supplemented with 0.5% PEST, and 2% Cellartis Hepatocyte Additives (Y11078, Takara Bio) in Costar 96 well ultra-low attachment plates (7007, Corning) with 30.000 cells per well in 100µl plating medium. 24 h post-seeding, medium was changed to 3D spheroid maintenance medium as described by Rashidi and colleagues (Rashidi et al. 2018). 24 - 48 h post-seeding, spheroids had formed and were maintained for up to 35 days with 50% medium changes every 2-3 days. Alternatively, spheroids could also be maintained with the 2D co-culture medium described above.

Cryopreserved hphep from three donors (Cat.no. M00995-P for male donors, F00995-P for female donors, BioIVT), selected based on high viability (see Table 1 for donor details), were thawed and plated according to the provider's instructions. For experiments that required the hepatocytes to be cultured for 24 h, medium was changed 4 hours post-plating to fresh Plating medium (InVitroGRO CP medium, BioIVT).

Transcriptomics analysis

Total RNA extraction

Two batches of Enhanced hiPS-HEP v2 from each hiPSC line (ChiPSC12, ChiPSC18, and ChiPSC22) were harvested on day 13 post-thawing by scraping the cells in the culture medium, centrifuging at 300g for 5 min and frozen as dry cell pellets. Human primary hepatocytes (n=3 donors) were harvested as dry cell pellets directly after thawing (day 0) and on day 1 post-thawing (day 1). Cell pellets were stored at -80 C until RNA extraction. Total RNA was extracted from the cell pellets using the GenElute RNA/DNA/protein Plus Purification kit (E5163, Sigma Aldrich). RNA amounts were quantified using a NanoDrop ND-1000 (NanoDrop, http://www.nanodrop.com).

Gene array

The quality of the RNA and cDNA was verified using a 2100 Agilent Bioanalyzer. To measure the mRNA levels, cDNA was synthesized from the RNA samples applying the GeneChip WT PLUS Reagent Kit (Affymetrix) and fragmented cDNA was hybridized at 45 degree Celsius for 16 hours to whole transcript HuGene ST 2.0 arrays (Affymetrix, http://www.affymetrix.com) at SCIBLU Genomics (Lund University, Sweden). In total 12 expression microarrays were run. Raw and processed data were submitted to ArrayExpress accession number: E-MTAB-8286.

Data processing

Raw microarray data was imported into R (R Core Team, 2017) and signal intensities normalized by the Robust Multichip Average method in the oligo package (Carvalho and Irizarry, 2010). The two biological replicates for each hiPSC line were summarized by mean expression. To remove transcripts with expression values close to background, probes with a log2 expression below 5 in all samples were removed. The resulting dataset contained 21,427 transcripts and 9 samples (3 hphep day 0, 3 hphep day 1, 3 hips-HEP). The transcripts were mapped to HGNC symbols using the HuGene 2.0 ST V1 NetAffx file from Affymetrix (NA36, genome build hg19). The microarray data used in this study follow the MIAME standard and raw expression data are available at ArrayExpress (https://www.ebi.ac.uk/arrayexpress/), accession number E-MTAB-8286.

Statistical analysis

Inspection of transcriptomics data revealed an approximate gamma distribution, and thus statistical testing for differential expression was based on a generalized linear model (GLM) from the gamma family with a linear link. The GLM was fitted using genes as response variables and sample group (hphep day 0, hphep day 1, hiPS-HEP) as covariates. The primary human hepatocytes day 0 and day 1 samples were treated as paired. Statistical significance of differential expression was

assessed with the likelihood ratio test. P-values were adjusted for multiple testing by Benjamini-Hochberg correction. Differentially expressed genes were identified using a combined criterion of adjusted $p < 0.05$ and absolute log2 fold change > 2.

Pathway over-representation analysis of the differentially expressed genes was carried out with Reactome Pathway Database [48, 49], using a criterion of a p-value < 0.05, and at least two differentially expressed genes present for the identified over-represented pathways.

Immunocytochemistry

Cells were stained as described previously (Ulvestad et al., 2013). Briefly, Enhanced hiPS-HEP v2 were fixed on day 12 post-thawing and hphep on day 1 post-thawing, by 15 min incubation with 4% Formaldehyde. Cells were stained with the following primary and secondary antibodies: rabbit anti-α1AT (A0012, DAKO, 1:200 dilution), rabbit anti-albumin (A0001, DAKO, 1:1000), mouse anti-ASGPR1 (MAI-40244, ThermoFisher 1:50), rabbit-anti-BSEP (purchased from Prof. Bruno Stieger, University Hospital Zurich, Switzerland, 1:100); rabbit anti-HNF4α (SC-8987, SantaCruz Biotechnology, 1:300), rabbit anti-MRP2 (SC-20766, SantaCruz Biotechnology, 1:50), rabbit anti-NTCP (Bruno Stieger, 1:400), rabbit anti-OATP1B1 (Bruno Stieger, 1:200), donkey anti-rabbit Alexa 594 IgG (A21207, Invitrogen, 1:1000) or goat anti-mouse Alexa 488 (A11029, Invitrogen, 1:1000). For nuclear counterstaining, DAPI (Sigma, D9542) was added during the incubation with the secondary antibodies (add 2µl/ml of a 1mg/ml DAPI stock in DMSO). Stainings were examined using an inverted fluorescence microscope (Eclipse Ti-U, Nikon), ANDOR Zyla sCMOS digital camera and the NIS-Elements software package (version 4.30). Technical control staining without primary antibodies were performed for all secondary antibodies and these were negative (data not shown). Quantification of HNF4α positive cells was done in relation to DAPI stained cells using the CellC Cell Counting Software [50].

Co-cultures of Enhanced hiPS-HEP v2 and HSC were permeabilized with 0.5% Triton X-100 solution in PBS for 1 h at room temperature (RT) and then incubated for 30 min at RT with blocking buffer containing 1% BSA and 10% normal goat serum (Sigma). Primary and secondary antibodies were diluted in blocking buffer. Cells were incubated for 2 h at RT (α-SMA) or overnight at 4°C (HNF4α) with the primary antibodies and subsequently washed three times with PBS before incubating with the secondary antibodies for 1 h at RT. Next, cells were washed three times with PBS, stained for 5 min with DAPI diluted 1:25.000 in PBS and washed again. The following primary and secondary antibodies were used: mouse anti-α-smooth muscle actin (α-SMA; 1:1.000; A5228, Sigma), mouse anti-HNF4α (1:200; ab41898, Abcam), goat anti-mouse Alexa Fluor 594 (1:300; ThermoFisher Scientific), and goat anti-mouse FITC (1:50; ThermoFisher Scientific). Fluorescent images were acquired on an Axio Observer Z1 Zeiss microscope (Zeiss, Breda, The Netherlands) and processed with ZEN 2.3 lite software (Zeiss).

Period acid-Schiff (PAS) staining

Glycogen storage was visualized by PAS staining of Enhanced hiPS-HEP v2 derived from C12, C18, and C22 (fixed on day 12 post-thawing) and hphep (fixed on day 1 post-thawing). Cells were stained with the glycogen assay kit (MAK016, Sigma) according to the manufacturer's protocol.

Albumin secretion

Albumin secretion from Enhanced hiPS-HEP v2 (derived from C12, C18, and C22) was analyzed on days 4, 6, 12, and 20 post-thawing and from hphep cells 24 h post-thawing. The culture medium was collected after 24 h of conditioning and Albumin content was analyzed with the Albuwell kit (Exocell, Philadelphia, PA) according to the manufacturer's protocol. The Albumin content in the medium was normalized to the assay duration (24 h) and the amount of protein per well.

For protein quantification, cells were washed once with DPBS (with Calcium and Magnesium) and lysed in 0.02 mM NaOH over night at 4°C and stored at -20°C until quantification using the

Pierce BCA Protein Assay kit (ThermoFisher, Rockford, IL) according to the manufacture's instruction.

Urea secretion

On days 13 and 20 post-thawing, Enhanced hiPS-HEP v2 and hphep d1 were incubated with 5 mM ammonium chloride for 24 h. After 24 h, medium was collected, and urea secretion was analyzed with the QuantiChrom Urea Assay Kit (BioAssay Systems, Hayward, CA). Urea content was normalized to the amount of protein per well (determined using the Pierce BCA Protein Assay Kit, see above) and the assay duration (24 h).

AKT Western Blot

Phosphorylated AKT: Enhanced hiPS-HEP (derived from C18, on day 12 post-thawing) were incubated in insulin-free medium (phenol-red free Williams' medium E containing 0.1% PEST, 25 mM HEPES, 2 mM L-Glutamine) for 3 h and then treated for 10 min with 0 nM or 100 nM insulin. Phosphorylated AKT (Cell Signaling) and total AKT (Cell Signaling) were quantified by Western blot (NuPAGE 4-12% Bis-Tris Protein Gels, Thermo Fisher Scientific).

CYP activity assay

The CYP activities of Enhanced hiPS-HEP v2 were analyzed by performing a CYP activity assay at days 4, 12, and 19 after thawing and the results were compared to hphep cultured for 20 hours. Briefly, the cells were carefully washed twice with pre-warmed Williams' medium E (Phenol-red free, + 0.1% PEST). Then, the activity assay was started by adding 110 µl/cm2 culture area of pre-warmed Williams' medium E (phenol-red free) containing 0.1% PEST, 25 mM HEPES (H7523, Sigma), 2 mM L-Glutamine, and the probe substrate cocktail (see Table 2 below). After a 2-hour incubation at 37°C, 100 µl of the supernatant was collected and kept at -80°C until LC/MS analysis. LC/MS analysis (performed at Pharmacelsus GmbH, Saarbrücken, Germany) was used to measure the formation of the specific metabolites Acetaminophen (CYP1A), OH-Bupropion (CYP2B6), 4-OH-Diclofenac (CYP2C9), 4-OH-Mephenytoin (CYP2C19), OH-Bufuralol (CYP2D6), and 1-OH-Midazolam (CYP3A). The metabolite concentrations were normalized to the amount of protein per well (determined using the Pierce BCA Protein Assay Kit, see above) and the assay duration (120 min). To be able to normalize the results between different LCMS runs, a metabolite cocktail with known concentrations of all metabolites is included in every analysis batch.

Table 2. CYP activity substrate cocktail

CYP	Substrate	Assay concentration
1A	Phenacetin	10µM
2B6	Bupropion	10µM
2C19	Mephenytoin	50µM
2C9	Diclofenac	10µM
2D6	Bufuralol	10µM
3A	Midazolam	5µM

Phase II enzyme activity assay

The phase II enzyme activities of Enhanced hiPS-HEP v2 were analyzed day 4, 8, 12, and 19 after thawing by performing a phase II activity assay. Briefly, the cells were carefully washed twice with pre-warmed Williams' medium E (+ 0.1% PEST). Then the activity assay was started by adding 110 µl/cm2 culture area of pre-warmed Williams' medium E containing 0.1% PEST, 25 mM HEPES, 2

738 mM L-Glutamine, and 200µM 7-OH-coumarin. After a 2-hour incubation at 37°C, 100 µl of the
739 supernatant was collected and kept at -80°C until LC/MS analysis. LC/MS analysis (performed at
740 Pharmacelsus GmbH) was used to measure the formation of 7-OH-coumarin sulfate and 7-OH-
741 coumarin glucuronide, specific metabolites for sulfotransferases and UDP-
742 glucuronosyltransferases, respectively. The metabolite concentrations were normalized to the
743 amount of protein per well (determined using the Pierce BCA Protein Assay Kit, see above) and the
744 assay duration (120 min).

745 ***LDL uptake***

746 In order to determine the uptake of low-density lipoproteins (LDL), Enhanced hiPS-HEP v2
747 (derived from C12, C18, and C22), on day 6 after thawing, were incubated for 3 h with LDL-
748 DyLight (Cat.no. 10011125, Cayman Chemical, Hamburg, Germany) diluted 1:100 in regular
749 maintenance medium. Next, cells were washed once with DPBS (with Calcium and Magnesium)
750 and immunofluorescence was recorded as described above under immunocytochemistry.

751 ***Fatty acid accumulation and inflammatory response***

752 Enhanced hiPS-HEP v2 were incubated for 24 h (on days 5-6 post-thawing) with Williams'
753 medium E containing 0.1% PEST, 25 mM HEPES, and 2 mM L-Glutamine supplemented with either
754 200µM oleic acid (OA, O1008, Sigma) coupled to 77µM fatty acid-free BSA (FAF-BSA, A8806, Sigma),
755 600 µM OA coupled to 231µM FAF-BSA, or only 231 µM FAF-BSA (as vehicle control). In addition,
756 one group of cells was treated with 200µM OA (coupled to 77µM FAF-BSA) plus 1µM Thapsigargin
757 (T0933, Sigma). After the 24 h incubation, cells were either stained with Oil Red O or harvested for
758 gene expression analysis. Oil Red O staining was performed using the Hepatic Lipid
759 Accumulation/Steatosis Assay Kit (Cat.no. ab133131, Abcam) according to the protocol provided
760 with the kit. Stainings were evaluated using a Zeiss AxioVert microscope, an Axicam 105 color
761 camera and the ZEN2 software (all from Carl Zeiss, Jena, Germany). For gene expression analysis,
762 cells were harvested in RNAprotect Cell Reagent (Cat No. 76526, Qiagen). RNA preparation, cDNA
763 synthesis, and qPCR were performed as described previously in Ulvestad et al, 2013. Gene expression
764 was analyzed using the TaqMan Gene Expression Assays (Applied Biosystems, Foster City, CA):
765 *TNFα* (Hs00174128_m1), and *CEBPα* (Hs00269972_s1) which served as a reference gene.

766 ***RNA prep and RT-qPCR of co-cultures and 3D spheroids***

767 Total RNA from co-cultures and from 3D spheroids was isolated using the Ambion RNAqueous
768 RNA Isolation Kit (ThermoFisher). The manufacturer's supplied protocol was followed during the
769 isolation and RNA concentrations were measured using the nanodrop ND-1000 spectrophotometer.
770 Cellular RNA (maximum of 200ng) was reverse transcribed into cDNA using the High Capacity RNA
771 to cDNA kit (Applied Biosystems) in a total reaction volume of 20µL consisting of 9µL assay buffer,
772 1µL enzyme mixture and added up to 20µL with RNAse free H2O. Samples were incubated for 60
773 minutes at 37°C and 5 minutes at 95°C using a BioRad iCycler. qPCR samples were subsequently
774 prepared by diluting cDNA samples 1:1 with RNAse free H2O and samples consisted of 2µL diluted
775 cDNA, 0.625µL assay on demand (AoD, ThermoFisher) or 25µM primers with 6.25 µL Taqman®
776 Gene expression mastermix (ThermoFisher) filled up to a total volume of 12.5µL with RNAse free
777 H2O. Samples were run at 50°C for 2 minutes, 95°C for 10 minutes and 40-45 cycles, each cycle
778 consisting of 95°C for 15 seconds and 60°C for 1 minute using the QuantStudio6 flex. The following
779 TaqMan Gene Expression Assays were used: *Collagen 1a1* (Hs01076777_m1), *Collagen 5a1*
780 (Hs00609133_m1), *HNF4α* (Hs00230853_m1), and *HPRT1* (Hs03929098_m1). The latter served as a
781 reference gene.
782

783 **Supplementary Materials:** Supplementary materials can be found at www.mdpi.com/xxx/s1.

784 **Supplemental Table 1:** see separate excel file.

Preprints (www.preprints.org) | NOT PEER-REVIEWED | Posted: 14 November 2019 doi:10.20944/preprints201911.0162.v1

Peer-reviewed version available at *Int. J. Mol. Sci.* **2020**, *21*, 469; doi:10.3390/ijms21020469

Supplemental Figure 1

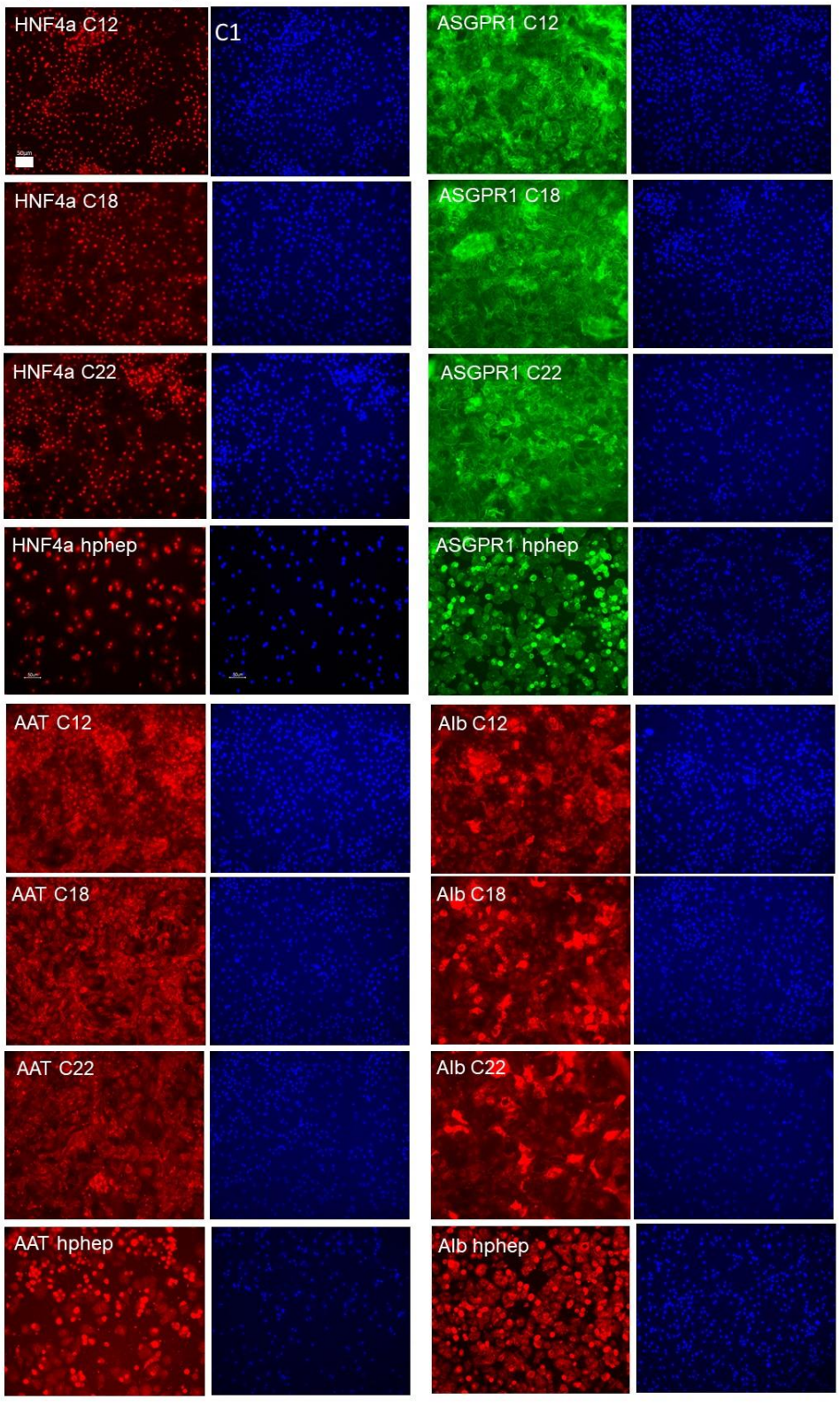

785

786 **Supplemental Figure 1** Representative pictures of immunocytochemical stainings of the hepatocyte markers
787 Hepatocyte Nuclear Factor 4α (HNF4α), Asialoglycoprotein receptor 1 (ASGPR1), α1-Antitrypsin (AAT), and
788 Albumin (Alb) in hiPS-HEP derived from ChiPSC12, ChiPSC18 and ChiPSC22, respectively, on day 12 post-
789 thawing and hphep cultured for 24 hours post-thaw. Scale bar 50µm.

Author Contributions: Conceptualization, A.A., R.H., B.K.-M., J.S.; methodology, A.A., B.K.-M., R.H.; software, B.U.; validation, A.A., K.T., A.H., B.K.-M.; formal analysis, G.H., B.U.; investigation, A.A., K.T., A.H., B.K.-M.; resources, C.X.A., R.H., J.S.; data curation, B.U., G.H.; writing—original draft preparation, A.A., B.K.-M., B.U., G.H; writing—review and editing, A.A., B.K.-M., B.U., G.H., K.T., C.X.A., A.H., R.H., J.S.; visualization, A.A., B.K.-M., B.U., G.H.; A.H., K.T., R.H.; supervision, J.S., B.K.-M., A.A., C.X.A., R.H.; project administration, J.S., B.K.-M., A.A., C.X.A., R.H.; funding acquisition, J.S., R.H.

Funding:

This work was supported by the Systems Biology Research Centre at University of Skövde under grants from the Knowledge Foundation [2014/0301, 2016/0293 and 2017/0302], and Takara Bio Europe, Gothenburg, Sweden.

Acknowledgments:

We are grateful to Roxana Khatib Shahidi at The Lundberg Laboratory for Diabetes Research (Department of Molecular and Clinical Medicine, Sahlgrenska Academy at the University of Gothenburg, Gothenburg, Sweden) and Paula Metselaar and Daan 't Hart at TNO for technical assistance.

Conflicts of Interest:

A.A., B.K.-M. and C.X.A. are employees at Takara Bio Europe. R.H. and K.T. are employees at TNO. The other authors declare no conflict of interest.

Abbreviations

AAT	α1-Antitrypsin
Alb	Albumin
ASGPR1	Asialoglycoprotein receptor 1
CYP	Cytochrome P450
DEGs	Differentially Expressed Genes
hiPSC	Human pluripotent stem cells
hiPS-HEP	hiPSC-derived hepatocytes
HNF4α	Hepatocyte Nuclear Factor 4 α
hphep	human primary hepatocytes
HSC	Hepatic Stellate Cells
NAFLD	Non-Alcoholic Fatty Liver Disease
NASH	Non-Alcoholic Steatohepatitis
OA	Oleic acid
TGFβ	Transforming Growth Factor β
TNFα	Tumor Necrosis Factor α

References

1. Byass, P., *The global burden of liver disease: a challenge for methods and for public health.* BMC Med, 2014. **12**: p. 159.
2. Goldring, C., et al., *Stem cell-derived models to improve mechanistic understanding and prediction of human drug-induced liver injury.* Hepatology, 2017. **65**(2): p. 710-721.
3. Guguen-Guillouzo, C. and A. Guillouzo, *General review on in vitro hepatocyte models and their applications.* Methods Mol Biol, 2010. **640**: p. 1-40.
4. Rodriguez-Antona, C., et al., *Cytochrome P450 expression in human hepatocytes and hepatoma cell lines: molecular mechanisms that determine lower expression in cultured cells.* Xenobiotica, 2002. **32**(6): p. 505-20.
5. Ulvestad, M., et al., *OATP1B1/1B3 activity in plated primary human hepatocytes over time in culture.* Biochem Pharmacol, 2011. **82**(9): p. 1219-26.
6. Ulvestad, M., et al., *Drug metabolizing enzyme and transporter protein profiles of hepatocytes derived from human embryonic and induced pluripotent stem cells.* Biochem Pharmacol, 2013. **86**(5): p. 691-702.

7. Messner, S., et al., *Multi-cell type human liver microtissues for hepatotoxicity testing.* Arch Toxicol, 2013. **87**(1): p. 209-13.
8. Schwartz, R.E., et al., *Pluripotent stem cell-derived hepatocyte-like cells.* Biotechnol Adv, 2014. **32**(2): p. 504-13.
9. Jungermann, K. and T. Kietzmann, *Zonation of parenchymal and nonparenchymal metabolism in liver.* Annu Rev Nutr, 1996. **16**: p. 179-203.
10. Heslop, J.A. and S.A. Duncan, *The Use of Human Pluripotent Stem Cells for Modeling Liver Development and Disease.* Hepatology, 2019. **69**(3): p. 1306-1316.
11. Parafati, M., et al., *A nonalcoholic fatty liver disease model in human induced pluripotent stem cell-derived hepatocytes, created by endoplasmic reticulum stress-induced steatosis.* Dis Model Mech, 2018. **11**(9).
12. Yamashita, T., et al., *Pharmaceutical Research for Inherited Metabolic Disorders of the Liver Using Human Induced Pluripotent Stem Cell and Genome Editing Technologies.* Biol Pharm Bull, 2019. **42**(3): p. 312-318.
13. Lyu, C., et al., *Targeted genome engineering in human induced pluripotent stem cells from patients with hemophilia B using the CRISPR-Cas9 system.* Stem Cell Res Ther, 2018. **9**(1): p. 92.
14. Omer, L., et al., *CRISPR Correction of a Homozygous Low-Density Lipoprotein Receptor Mutation in Familial Hypercholesterolemia Induced Pluripotent Stem Cells.* Hepatol Commun, 2017. **1**(9): p. 886-898.
15. Ohtsuki, S., et al., *Simultaneous absolute protein quantification of transporters, cytochromes P450, and UDP-glucuronosyltransferases as a novel approach for the characterization of individual human liver: comparison with mRNA levels and activities.* Drug Metab Dispos, 2012. **40**(1): p. 83-92.
16. Oseini, A.M. and A.J. Sanyal, *Therapies in non-alcoholic steatohepatitis (NASH).* Liver Int, 2017. **37 Suppl 1**: p. 97-103.
17. Wells, R.G., *The role of matrix stiffness in hepatic stellate cell activation and liver fibrosis.* J Clin Gastroenterol, 2005. **39**(4 Suppl 2): p. S158-61.
18. Asplund, A., et al., *One Standardized Differentiation Procedure Robustly Generates Homogenous Hepatocyte Cultures Displaying Metabolic Diversity from a Large Panel of Human Pluripotent Stem Cells.* Stem Cell Rev, 2016. **12**(1): p. 90-104.
19. Kajiwara, M., et al., *Donor-dependent variations in hepatic differentiation from human-induced pluripotent stem cells.* Proc Natl Acad Sci U S A, 2012. **109**(31): p. 12538-43.
20. Hannan, N.R., et al., *Production of hepatocyte-like cells from human pluripotent stem cells.* Nat Protoc, 2013. **8**(2): p. 430-7.
21. Peters, D.T., et al., *Asialoglycoprotein receptor 1 is a specific cell-surface marker for isolating hepatocytes derived from human pluripotent stem cells.* Development, 2016. **143**(9): p. 1475-81.
22. Mitchell, S., et al., *Genetic variation in the urea cycle: a model resource for investigating key candidate genes for common diseases.* Hum Mutat, 2009. **30**(1): p. 56-60.
23. Zanger, U.M. and M. Schwab, *Cytochrome P450 enzymes in drug metabolism: regulation of gene expression, enzyme activities, and impact of genetic variation.* Pharmacol Ther, 2013. **138**(1): p. 103-41.
24. Zanger, U.M., et al., *Functional pharmacogenetics/genomics of human cytochromes P450 involved in drug biotransformation.* Anal Bioanal Chem, 2008. **392**(6): p. 1093-108.
25. Jancova, P., P. Anzenbacher, and E. Anzenbacherova, *Phase II drug metabolizing enzymes.* Biomed Pap Med Fac Univ Palacky Olomouc Czech Repub, 2010. **154**(2): p. 103-16.
26. Richert, L., et al., *Evaluation of the effect of culture configuration on morphology, survival time, antioxidant status and metabolic capacities of cultured rat hepatocytes.* Toxicol In Vitro, 2002. **16**(1): p. 89-99.

27. Richert, L., et al., *Gene expression in human hepatocytes in suspension after isolation is similar to the liver of origin, is not affected by hepatocyte cold storage and cryopreservation, but is strongly changed after hepatocyte plating.* Drug Metab Dispos, 2006. **34**(5): p. 870-9.
28. den Braver-Sewradj, S.P., et al., *Inter-donor variability of phase I/phase II metabolism of three reference drugs in cryopreserved primary human hepatocytes in suspension and monolayer.* Toxicol In Vitro, 2016. **33**: p. 71-9.
29. Hewitt, N.J., et al., *Primary Hepatocytes: Current Understanding of the Regulation of Metabolic Enzymes and Transporter Proteins, and Pharmaceutical Practice for the Use of Hepatocytes in Metabolism, Enzyme Induction, Transporter, Clearance, and Hepatotoxicity Studies.* Drug Metabolism Reviews, 2007. **39**(1): p. 159-234.
30. Smith, C.M., et al., *A comprehensive evaluation of metabolic activity and intrinsic clearance in suspensions and monolayer cultures of cryopreserved primary human hepatocytes.* J Pharm Sci, 2012. **101**(10): p. 3989-4002.
31. Smith, B.C., et al., *Differences in 2-oxoglutarate dehydrogenase regulation in liver and kidney.* Biochem J, 1992. **284 (Pt 3)**(Pt 3): p. 819-26.
32. Kietzmann, T., *Metabolic zonation of the liver: The oxygen gradient revisited.* Redox Biol, 2017. **11**: p. 622-630.
33. Ratziu, V., et al., *A position statement on NAFLD/NASH based on the EASL 2009 special conference.* J Hepatol, 2010. **53**(2): p. 372-84.
34. Sanyal, A.J., et al., *Endpoints and clinical trial design for nonalcoholic steatohepatitis.* Hepatology, 2011. **54**(1): p. 344-53.
35. Starley, B.Q., C.J. Calcagno, and S.A. Harrison, *Nonalcoholic fatty liver disease and hepatocellular carcinoma: a weighty connection.* Hepatology, 2010. **51**(5): p. 1820-32.
36. Feaver, R.E., et al., *Development of an in vitro human liver system for interrogating nonalcoholic steatohepatitis.* JCI Insight, 2016. **1**(20): p. e90954.
37. Boeckmans, J., et al., *Human-based systems: Mechanistic NASH modelling just around the corner?* Pharmacol Res, 2018. **134**: p. 257-267.
38. Nilsson, S.K., et al., *Endocytosis of apolipoprotein A-V by members of the low density lipoprotein receptor and the VPS10p domain receptor families.* J Biol Chem, 2008. **283**(38): p. 25920-7.
39. Fang, D.L., et al., *Endoplasmic reticulum stress leads to lipid accumulation through upregulation of SREBP-1c in normal hepatic and hepatoma cells.* Mol Cell Biochem, 2013. **381**(1-2): p. 127-37.
40. Ratziu, V., et al., *Elafibranor, an Agonist of the Peroxisome Proliferator-Activated Receptor-alpha and -delta, Induces Resolution of Nonalcoholic Steatohepatitis Without Fibrosis Worsening.* Gastroenterology, 2016. **150**(5): p. 1147-1159.e5.
41. Abenavoli, L., et al., *Obeticholic Acid: A New Era in the Treatment of Nonalcoholic Fatty Liver Disease.* Pharmaceuticals (Basel), 2018. **11**(4).
42. Kanuri, G. and I. Bergheim, *In vitro and in vivo models of non-alcoholic fatty liver disease (NAFLD).* Int J Mol Sci, 2013. **14**(6): p. 11963-80.
43. Graffmann, N., et al., *Modeling Nonalcoholic Fatty Liver Disease with Human Pluripotent Stem Cell-Derived Immature Hepatocyte-Like Cells Reveals Activation of PLIN2 and Confirms Regulatory Functions of Peroxisome Proliferator-Activated Receptor Alpha.* Stem Cells Dev, 2016. **25**(15): p. 1119-33.
44. Miyoshi, M., et al., *LIM homeobox 2 promotes interaction between human iPS-derived hepatic progenitors and iPS-derived hepatic stellate-like cells.* Sci Rep, 2019. **9**(1): p. 2072.

45. Koui, Y., et al., *An In Vitro Human Liver Model by iPSC-Derived Parenchymal and Non-parenchymal Cells.* Stem Cell Reports, 2017. **9**(2): p. 490-498.
46. Coll, M., et al., *Generation of Hepatic Stellate Cells from Human Pluripotent Stem Cells Enables In Vitro Modeling of Liver Fibrosis.* Cell Stem Cell, 2018. **23**(1): p. 101-113.e7.
47. Ölander, M., et al., *A simple approach for restoration of differentiation and function in cryopreserved human hepatocytes.* Archives of Toxicology, 2019. **93**(3): p. 819-829.
48. Fabregat, A., et al., *The Reactome Pathway Knowledgebase.* Nucleic Acids Res, 2018. **46**(D1): p. D649-d655.
49. Fabregat, A., et al., *Reactome pathway analysis: a high-performance in-memory approach.* BMC Bioinformatics, 2017. **18**(1): p. 142.
50. Selinummi, J., et al., *Software for quantification of labeled bacteria from digital microscope images by automated image analysis.* Biotechniques, 2005. **39**(6): p. 859-63.